5-2012

Physiochemical and Nanomanipulation Studies of Carbon Nanomaterials

Siva Naga Sandeep Chalamalasetty
University of Arkansas, Fayetteville

PHYSIOCHEMICAL AND NANOMANIPULATION STUDIES OF CARBON NANOMATERIALS

PHYSIOCHEMICAL AND NANOMANIPULATION STUDIES OF CARBON NANOMATERIALS

A thesis submitted in partial fulfillment
of the requirements for the degree of
Master of Science in Microelectronics-Photonics

By

Siva Naga Sandeep Chalamalasetty
Andhra University
Bachelor of Technology in Biotechnology, 2008

May 2012
University of Arkansas

ABSTRACT

Carbon nanomaterials are, without a doubt, one of man's wonder creations. Though these nanomaterials are a very recent trend, extraordinary electromechanical properties and the light weightiness of these nanomaterials attracted the attention of researchers. Although vast research has been done since the start of the US nanotechnology initiative, much effort was in the area of synthesis and characterization of the nanomaterials. However, most of the traditional macroscopic material's theories fail at the nanoscale level, and since the material properties are dependent on size and structure at nanoscale level, the behavior of the carbon nanomaterials in different environments needs attention. High tensile strength and high tensile modulus with low weight make these nanomaterials ideal for light weighted structures. Thus, many space organizations like NASA are conducting research on these exciting nanomaterials. Hence, dimensional changes of carbon nanofibers in the ambient and subzero temperature ranges was quantified and statistically analyzed. Mechanical properties of the carbon nanofibers both at room temperature and in subzero temperature range was measured using AFM based nanoindentation. Inability to control the orientation of the nanomaterials and lack of material integration to substrate were the primary causes for selecting synthesis over deposition even though the former is a cumbersome process. The challenge of nanomaterials integration to substrates can be mitigated by synthesis of nanocomposites, which are hybrid materials with enhanced electromechanical properties and better substrate integration, and the challenge of orientation can be mitigated by nanopatterning i.e., creating the channels using AFM based picolithography. These methods were demonstrated in this thesis.

This thesis is approved for recommendation

to the Graduate Council.

Thesis Director:

_____

Dr. Uchechukwu C. Wejinya

Thesis Committee:

_____

Dr. Kaiming Ye

_____

Prof. Ken Vickers

The following signatories attest that all software used in this thesis was legally licensed for use by Mr. Siva Naga Sandeep Chalamalasetty for research purposes and publication.

_____	_____
Mr. Siva Naga Sandeep Chalamalasetty Student	Dr. Uchechukwu C. Wejinya Thesis Director

This thesis was submitted to http://www.turnitin.com for plagiarism review by the TurnItIn company's software. The signatories have examined the report on this thesis that was returned by TurnItIn and attest that, in their opinion, the items highlighted by the software are incidental to common usage and are not plagiarized material.

_____	_____
Prof. Ken Vickers Program Director	Dr. Uchechukwu C. Wejinya Thesis Director

THESIS DUPLICATION RELEASE

I hereby authorize the University of Arkansas Libraries to duplicate this thesis when needed for research and/or scholarship.

Agreed _____

Siva Naga Sandeep Chalamalasetty

Refused _____

Siva Naga Sandeep Chalamalasetty

ACKNOWLEDGEMENTS

Firstly, I would like to thank Dr. Uche Wejinya for his strong commitment and best mentoring throughout my work. I would also like to thank Prof. Ken Vickers and Ms. Renee for keeping me on track and guiding me to achieve my goals and making sure that I comply with all the university requirements in a timely manner. I would also like to thank Dr. Kaiming Ye and Dr. Ryan Tian for being part of my thesis committee and providing me inputs to bring out my best effort. I sincerely acknowledge Zhuxin Dong, Ph.D student MEEG for all his support rendered throughout the two years of our association. Research possible through the use of the High Density Electronics Center at the University of Arkansas, Fayetteville campus.

I would like express my sincere gratitude to Dr. Meyya Meyyappan, Dr. Jessica Koehne and Dr. Prabhu Armugam of NASA Ames Research Center for supplying me with the fabricated chips that are required for my experiments. I would like to thank Dr. Steve Tung and his lab, Dr. Fisher Yu and his lab, Dr. Kaiming Ye and his lab for providing valuable resources that helped me to complete my project successfully. I would like to thank both Chemistry and Physics department for supporting me through Assistantships through the last two years which have helped me to complete my education effortlessly. This project was financially supported by Arkansas Space Grant under Grant No. SW19025 and by University of Arkansas College of Engineering External Mentoring Award Program under Grant No. 0112 16092-17-000. Any opinions, findings, and conclusions or recommendations expressed in this material are those of the author and do not necessarily reflect the views of the funding agencies

Finally I would like to thank my Parents, sister and brother in law, and all my relatives who motivated me to pursue higher education and kept me enthusiastic throughout the pursuit.

DEDICATION

Dedicated to My Cute Little Niece for the Smiles She Brought in My Life

TABLE OF CONTENTS

LIST OF FIGURES

LIST OF TABLES

1. INTRODUCTION

1.1 Review on Nanotechnology

Throughout history, alchemists envisioned of building better materials that are stronger, lighter, and more durable coupled with better electrical and thermal properties. With the advent of Nanotechnology, their dream came true. Though Nanotechnology was a late born baby in the field of science, it had already created tremors by expanding its horizons in the fields of Electronics, Mechanics, Physics, Biology, Engineering, Chemistry, etc. [1-10]. Factors like better control of building an atomic lattice structure [11-12], and the possibility of manipulation at the atomic and sub atomic levels [13-14] made this an astounding and enticing field. Looking back into the history, even though the fundamentals of Nanotechnology were defined back in the 18^{th} century, it all began in the late 1980s with two ground breaking discoveries that set platform for this exotic field. The first major breakthrough came in the year 1985, when a group led by *Kroto et al* discovered the Buckminster fullerene [15], a C_{60} carbon compound followed by *Iijima et al,* [16], when they accidentally discovered that carbon nanomaterials are synthesized during arc discharge of fullerene (C_{60} compound). Inspired by this ignition, material researchers around the world had worked on a variety of materials and reported their nanostructures. Based on the structure, nanomaterials are classified as cylindrical Nanowires as in the case of Zinc Oxide (ZnO) [17] and Silicon (Si) [18], Nanoribbons as in Graphene (C chain) [19], hemisphere over cylinder shaped Nanofibers like the Carbon Nanofibers [20], Hallow Nanotubes like Single Wall and Multi Wall Carbon Nanotubes [21-22], Spherical Nanoparticles [23-28] like Gold (Au), Silver (Ag), Aluminum (Al), Diamond (C), Cobalt (Co), Nickel (Ni), etc., and Quantum Dots [29 - 30]. In all, without doubt one can consider Nanotechnology as a wonder of the 20^{th} century.

1.2 Review on Carbon Nanofibers

As mentioned in the previous section, Nanotechnology was initiated with the discovery of carbon nanomaterials. The earliest unverified discovery of carbon nanofibers was in the late 18^{th} century. A patent on filamentous carbon material was filed in 1889 [31]. Despite the high probability that this early material was a carbon nanofiber, the lack of proper tools (such as the high resolution microscopy) and proper communication, made this observation go unnoticed. The first scientific document containing the images of carbon nanomaterials was published in 1952 by physicists L.V. Radushkevich and V.M. Lukyanovich in Soviet journal of Physical Chemistry [32]. But this document was unnoticed by the Western world due to the limited technology transfer during the Cold War period. Research conducted during the 1950s showed growth of filamentous carbon on metal surfaces using a variety of carbon sources. Though much research until the 1980s explored different combinations of metals and a variety of carbon sources, the first major breakthrough came in 1985 when a group led by *Kroto et al.* discovered the compound Buckminster fullerene [16], a pure carbon C_{60} compound. A fullerene can take a shape of a sphere, tube or ellipsoid. Until the discovery of fullerene, only two carbon allotropes are known to the scientific community namely diamond and graphite. However, after the discovery of Buckminster fullerene (C_{60}), a variety of carbon allotropes came into existence. Figure 1.1 shows the structural images of carbon allotropes known to the scientific community as of today. As seen from the Figure 1.1, fullerenes are regular arrangement of penta and hexa carbon rings just like the surface of a football.

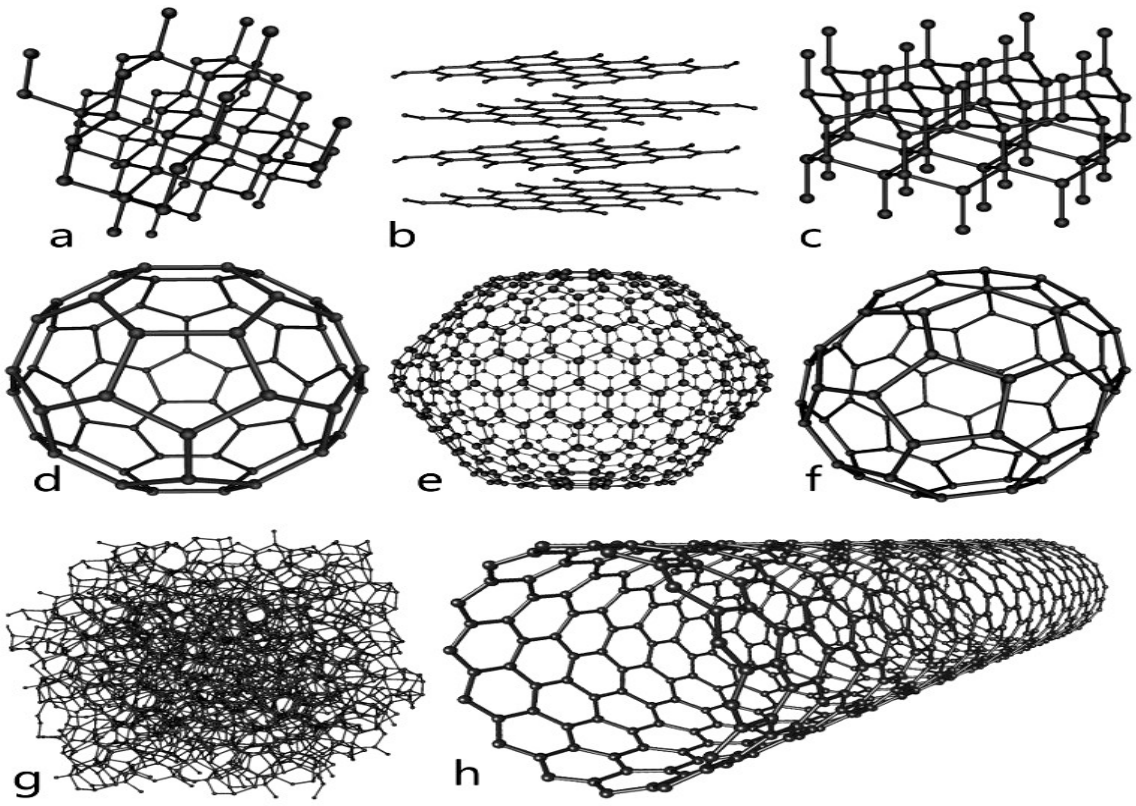

Figure 1.1. The structures of eight allotropes of carbon: a) Diamond b) Graphite c) Lonsdaleite d) C_{60} (Buckminsterfullerene) e) C_{40} Fullerene f) C_{70} Fullerene g) Amorphous carbon h) Single-walled carbon nanotube. A wonderful image released by Michael Ströck under the GNU Free Documentation License [33]

The discovery by Kroto et al was followed by the discovery by Iijima [17] in 1991 which conceded carbon nanotubes are produced during arc discharge of C_{60}. This discovery about the nanotubes brought awareness within the scientific community as a whole.

1.3 Properties of Carbon Nanofibers

Looking at the history of the nanomaterials, and knowing that over 16.5 billion US dollars has already been invested [34] by the US alone since the start of nanotechnology initiative in 2001, for the research of carbon nanomaterials one question immediately comes to the mind: Why is carbon nanomaterial so special to invest so much money on research of this

material? Looking at the properties of this material will give the answers. Nanotubes have been constructed with a length to diameter ratio of 132,000,000:1 which is significantly larger than any other known material [35]. It is the strongest and stiffest material discovered to date in terms of tensile strength and Young's modulus. With a Young's modulus and Tensile strength of ~ 1 Tpa [36] and 150 Gpa [37] respectively, they are almost 100 times stronger and stiffer than steel. Theoretically, carbon nanotubes (CNTs) can carry a current density of 4×10^9 A/ cm^3 which is almost 1000 times that of copper [38]. Thus, there won't be any material that is at least close to the carbon nanomaterials in terms of mechanical and electrical properties as of today.

1.4 Atomic Force Microscopy (AFM)

Invented in 1985 [39], AFM has become a major research tool for micro and nanoscale studies. With the basic principle relying on Hooke's law, AFM has the capability of measuring fractions of nanometer with a resolution upto 0.02 nm RMS. A cantilever containing the probe tip is brought in close proximity of the sample surface, where forces between the cantilever and sample cause a deflection on the cantilever and the force of deflection is recorded with the help of a piezoelectric scanner. Figure 1.2 shows the overall mechanism of the working of AFM and the cantilever with tip. As shown in the Figure 1.2, a laser beam is focused at the end of the cantilever on the top side and any deflection in the cantilever results in a deflection of laser beam which is recorded by the photodiode. In order to avoid the breakage of the tip, it is operated by a force feedback control and computer interface. Starting as an instrument to scan the topographies of nanoscale structures, now AFM is being used for studying mechanical contacts, Van der waal's and capillary forces, chemical bonding, electrical and magnetic properties, temperature distribution, etc.

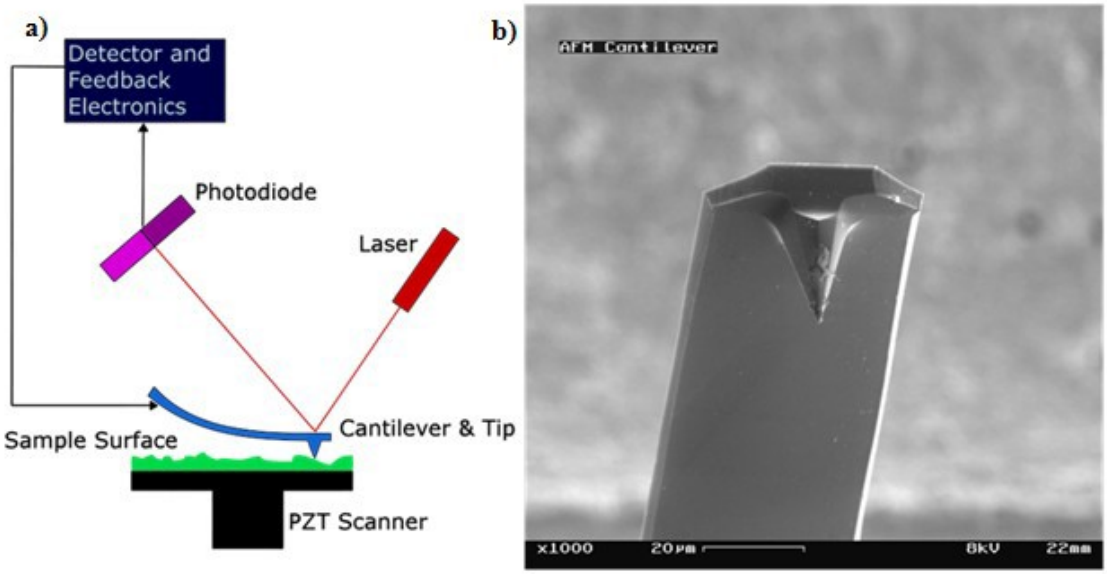

Figure 1.2. Atomic Force Microscopy. a) Schematic of AFM. b) An AFM Cantilever with the probe tip scanned using scanning electron microscope. Images retrieved and used under the Creative Commons Attribution-Share Alike 3.0 Unported license.

The amazing capability of this instrument is further enhanced by its ability to generate 3D images from the scanned images and its ability to scan in different modes like contact, intermittent contact or tapping, lateral force microscopy, phase imaging and non-contact mode. It can be used for almost any material with minimal sample preparation and without affecting the system integrity. But it has a disadvantage over the Scanning Electron Microscopy in terms of maximum scan size. While the SEM can be used to scan the images of square millimeters with a depth of field in millimeters, the maximum scan height of AFM is about 10-20 μm and it can generate only images of only 150 μm × 150 μm. The AFM can also be affected by the hysteresis of the piezoelectric material.

1.5 Conclusion

Materials of Nanotechnology will revolutionize the future and improve the standard of living of the present and future generations. A better understanding of them will provide more opportunity for better embedding and integration technologies.

2. OBJECTIVES AND MOTIVATIONS

2.1 Introduction of the objectives

Chip integration techniques of nanomaterials on silicon surfaces include a) direct growth of nanomaterial on the silicon substrate through fabrication techniques or b) deposition of nanomaterial on the silicon surface. Both methods have their own advantages and disadvantages. While the direct growth method has the orientation, size and purity control; the deposition method has the flexibility of easy integration and minimal equipment requirement. But both methods do have their own disadvantages. While the direct growth method needs cumbersome processing methodologies and involves treatment of many chemicals, deposition methods don't have orientation control.

At macroscale, device properties are functions of the geometry and the property of the material. The same principle can't be applied at the micro and nanoscale without modifications. For instance, carbon nanotubes electrical and mechanical properties are directly dependent on size and chirality [40-41]. Apparently at nanoscale, material properties and device geometry cannot be separated. Thus, a much complex system needs to be analyzed. Though many predicted the behavior of materials at nanoscale using atomistic computational models [42-49], no significant research was done in practice to verify these hypotheses. Hence using Taguchi's approach in this work, the temperature effect on vertically aligned carbon nanofibers was studied in detail.

Carbon nanomaterials have been proven to be excellent sensor materials [50-56]. With the advent of carbon nanomaterials, the dreams of chemists and biologists of detecting down to a single molecule can be made possible. Organizations such as NASA are exploring the possibility

of integrating these sensors to satellites and other space explorers to collect data precisely and accurately. The mission statement of NASA Ames Research center is stated below:

"To develop Nanotechnology based chemical sensors that can provide high sensitivity, low power and low cost portable tools for in-situ chemical analysis in space and terrestrial applications. Our generic nanosensor platform is suitable for detection of gases and volatile organic compounds. This platform can be used for chemical analysis in gas phases, and can also be extended for use in liquid phases." [57]

From the statement above it can be assumed that carbon nanofiber based sensors will be part of futuristic space missions. But in order to fortify nanofiber chips in space missions, one must make sure these sensors do not fail in the extreme environments of outer space. NASA in its report *"Extreme environment technologies for futuristic space missions"* identified pressure, temperature and radiation as three critical factors leading to the failure of their space missions. Below is a statement retrieved from the 2008 NASA report.

James A Cutts, Chief Technologist, Solar System Exploration Programs Directorate and Manager, NASA Planetary Program Support Task in his foreword for extreme environmental technologies for future space science missions a report released in 2008 said "*At this time, however, there is no program within SMD that directly supports development of the needed technologies by NASA centers, universities, and industries not qualifying for the SBIR program. This report should play an important role in documenting the need for new technology investments and in supporting the formulation of a coherent program to address extreme environment technology needs."* [58]

The above two statements acknowledge that there is still a lack of fundamental understanding of behavior of the carbon nanomaterials in extreme environments. Thus, this study aimed to understand the behavior of Carbon nanomaterials such as carbon nanofibers in harsh environments.

A composite material is a combination of two or more individual elements [59] that when combined gives enhanced properties. Composite materials were well researched at the macroscale but no significant research was done at micro and nanoscales. Building a composite material at micro and nanoscale is more interesting and challenging, as it needs manipulation down to atom scale. After the first successful development of nanocomposite, many developed a variety of nanocomposites using ceramics, metal particles, polymer matrix, etc., with carbon nanofibers [60-64]. Even though Carbon Materials are materials with excellent mechanical and electrical properties, their properties can be further enhanced with preparation of composite materials. Conductive polymers are a class of polymers that were extensively used in the development of solar cells since 1999. A variety of composites at macroscale have been successfully developed using conductive polymers [62]. But little work has been done at micro and nanoscales. Hence, a new breed of nanocomposites were developed using the combinations of conductive polymers and carbon nanotubes.

Metals are supposedly the best electric conductors because of their low resistivity. In general, a decrease in the material dimension will result in an increase in its overall resistance. For instance, looking at the conductance of the materials in macro and microscales it can be inferred that the material conductivity decreases by 100,000 fold when it comes to microscale and a billion fold in nanoscale provided the material internal properties don't change. But in the micro and nanoscale, material properties are no longer independent of particle size and

orientation resulting in more complexity of the system. Another major problem with some metals is that they oxidize and get rusted easily. A comprehensive solution for this problem is to find a material that can enhance the conductive properties while acting as a protective layer. Hence, in the present work CNT nanocomposites are coated onto the copper electrode.

With chip designing, manufacturing and patterning shrinking their sizes into nanoscale, it is of pivotal importance to develop new machines or upgrade the existing ones to perform multitasks. With the help of AFM, nanochannels can be scribed on the surface of a substrate. This is an added advantage of AFM and it can be used to create nanochannels. Depths of these nanochannels created with respect to a particular tip are studied in this work.

For achieving the goals described above, three different types of chips was fabricated using facilities at NASA Ames Research Center and the High Density Electronics center at the University of Arkansas, with fabrication procedures detailed in the following sections. An Environmental Chamber, a Nikon advanced fluorescent imaging microscope, a Philips SEM and an Agilent 5500 AFM were utilized for scan studies of the nanomaterials. All the chemicals used were bought from Sigma Aldrich and BDH.

2.2 Fabrication of the VACNF array chips

NASA Ames Research Center supplied the Vertically Aligned Carbon Nanofibers (VACNFs) Nano Electrode Arrays (NEA) and it included six major steps done on a 100 mm silicon (100) wafer that was previously coated with 500 nm of silicon dioxide. The fabrication process is shown in Figure 2.1, and the steps included A) metal deposition and patterning; B) Nano-patterning of Ni catalyst dots; C) directional growth of CNFs; D) silicon dioxide deposition for electrical isolation and mechanical support; E) chemical mechanical polishing

(CMP) to expose CNF tips and F) a wet etch with 7:1 HF. The overall fabrication procedure used in this process is given in Appendix H.

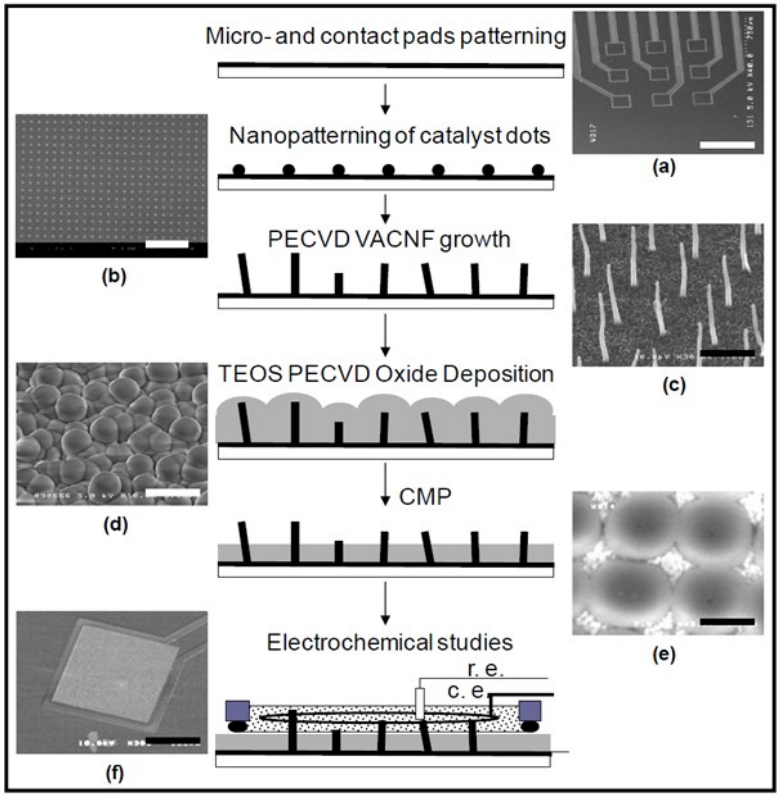

Figure 2.1 The fabrication steps and the changes on the wafer can be seen in the pictures in-sight. a) Deposition of metal, b) Nanopatterning, c)Growth of CNF's, d) Deposition of Silicon Dioxide and e) Chemical Mechanical Polishing.

2.3 Fabrication of Microelectrode Array Chip

Microelectrode Array chips, used for the studies of deposition methods and nanoscribing, were fabricated using our Hi-Density Electronics Center. The overall schematic showing the steps involved in the fabrication process are shown in Figure 2.2, and are detailed below:

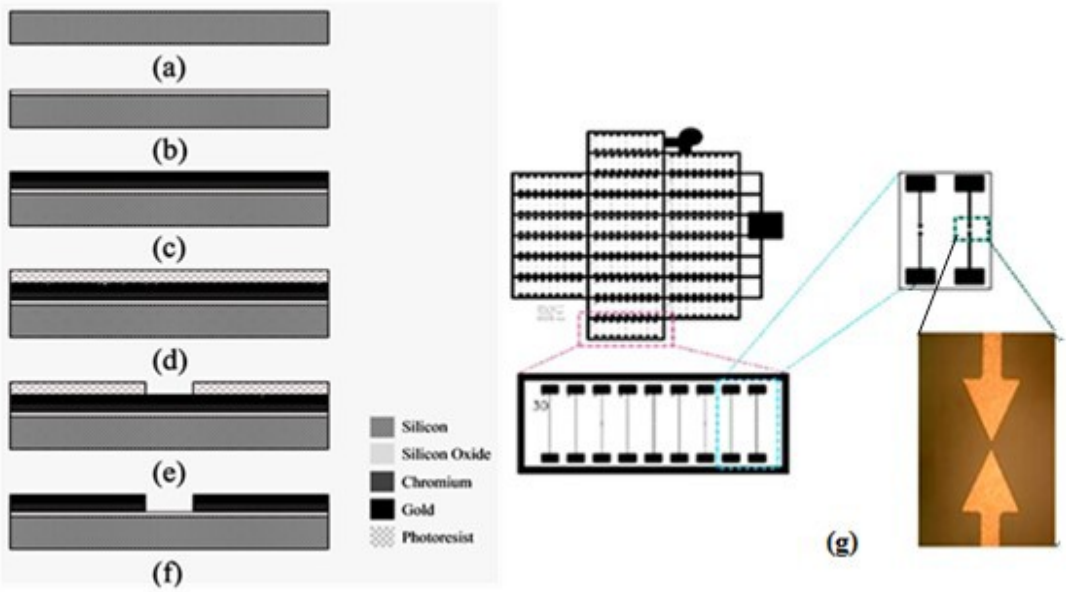

Figure 2.2. Fabrication Process of a Microelectrode. a) Si layer b) 500 A Silicon dioxide layer by thermal oxide deposition c) both chromium and gold deposited on silicon dioxide with evaporation d) cover the surface by photoresist e) photolithography and pattern f) wet etching and resist stripoff g) Mask Design and Gold Electrodes on Si substrate as Microelectrode

2.3.1 Oxidation of Silicon Wafer

A p-type Si wafer with <110> orientation was oxidized using the furnace at 1100^{o}C for 30 min (dry oxidation) and at 800^{o}C for 8 hours and cooled back to room temperature. A furnace method was the best way to grow Silicon Dioxide (SiO_2). In all, the above process resulted in about 500 Å of silicon dioxide. But the major problem with this method was oxide was grown both on top and bottom of the substrate. So an additional step was needed for back oxide removal. Photoresist was applied on the top, exposed and the back oxide was etched off using HF solution and the exposed photoresist was then removed.

2.3.2 Metal Deposition

Layers of chromium and gold were evaporated sequentially using the Evaporator. The wafer was mounted in the evaporator, and the chamber was vacuum pumped to a pressure of 1×10^{-5} mBar. Chromium and Gold electrodes were loaded into the crucibles and current was used to generate the heat required for the evaporation. At first, a screen was used in order to avoid the contamination and achieve steady rate of deposition. Then, the screen was lifted and the metal was deposited onto the substrate. A layer of 100 Å thick chromium and a layer of 500 Å gold were deposited. Gold has affinity towards Chromium but no affinity towards Silicon or Silicon Dioxide. Thus, a layer of Chromium was deposited prior to the deposition of Gold. While Chromium was evaporated at current of 3 A and at a rate of 2 Å/sec, Gold was evaporated at current of 2 A and at a rate of 3 Å/sec.

2.3.3 Patterning using Photolithography

Photoresist of thickness 3 µm was applied and then mask was imprinted onto the substrate using photolithography techniques. UV light was used to pattern the substrate with mask and substrate separated by 65 µm distance. The mask design used in the photolithography was shown in Figure 2.2(g). After the photolithography, the substrate was developed to remove the unexposed photoresist and thus complete the transfer of pattern onto the photoresist.

2.3.4 Metal Etch

Both Gold and Chromium were etched using Transene gold etchant and chrome etch respectively and this completed the patterning of the substrate. Now, the features were imprinted on the Silicon substrate as Gold/Chromium layers.

2.3.5 Resist Stripoff

The final step in the fabrication process was the resist stripoff. For this, the substrate was exposed to the UV light for about 30 seconds with no mask in order to complete the exposing of any unexposed photoresist and then it was developed to remove the photoresist. This completed the fabrication of the microelectrode arrays, with the final fabricated single microelectrode array was shown in the inset of Figure 2.2(g)

2.4 Conclusion

Motivations for the current work were discussed in detail and the plan of action was described. Wafer fabrication was carried out to develop the chips of different kinds. In all, two different types of chips were used in the current experimentation. Detailed fabrication procedures along with the process flow were shown and were carried out.

3. TEMPERATURE EFFECT ON THE VERTICALLY ALIGNED CARBON NANOFIBERS

3.1 Accelerated Aging Study on Carbon Nanofibers

Gregory Guisbiers et al [65], based on their studies on silicon tetrahedral nanoparticles, generalized that nanomaterials dimensions are effected by temperature and gave a general equation for change in the dimension of the nanomaterials with respect to changes in temperature which is shown in Equation (3.1).

$$\frac{T_x}{T_{x,\infty}} = \left(1 - \frac{\alpha}{D}\right)^{s-\frac{1}{2}} \qquad \text{Equation (3.1)}$$

Where T_x is surface temperature, $T_{x,\infty}$ is bulk temperature, α is height, D is diameter and s is spin number.

But Guisbiers team's work was in the range of super conductive, Debye, Curie and melting point temperatures and can't account for the dimensional dependency of the fibers on the temperature in the ambient temperature zone. An accelerated aging study is a standard laboratory technique used to study the durability of the material when there is no existing life span data for the material. Taguchi's approach is a widely accepted statistical method for technical studies to identify major effects and thus we adapted this method for statistical variance. Temperature impact on the dimensions of carbon nanofibers was studied, and any change in the dimensional data was recorded using atomic force microscopy. The detailed experimental procedure is given in the Section 3.2.

3.2. Experimental Setup

The fabricated unetched and HF etched Vertically Aligned Carbon Nanofiber (VACNF) nano electrode array chips were treated in the environmental chamber for 30 minutes at a constant 10% Relative Humidity (RH) with varying temperatures between 0^{o}C and 100^{o}C. They were then cooled back to room temperature and dried in the dry box until their relative humidity value fell below 3% RH. The cooled substrate chips were then scanned for changes in dimensions using atomic force microscope (Agilent 5500 SPM, Agilent Technologies, Inc., Santa Clara, CA, US)

A small scanner with Aluminum (Al) coated tip was used for scanning the samples. The tip had a force constant (F_c) of 48 N/m and a resonant frequency of 190 KHz. Prior to the experimentation, the tip sensitivity was calculated. Sensitivity (S) of the tip was the ratio of deflection of cantilever to the applied amplitude. The tip was calibrated for sensitivity with respect to mica surface and the tip sensitivity was 66.4 nm/V. A setpoint voltage (V) of 0.4V was used for the temperature study. Thus the applied tip force was 1.2 µN as calculated using Equation (3.2). The scanning was done in AC mode i.e., tapping mode, in order to protect the integrity of the chip. The overall experimental setup was shown in Figure 3.1. As shown in the Figure 3.1, the chip contained 9 electrode arrays and was loaded onto the sample holder and then onto the AFM.

$$F_{tip} = S * F_C * V \qquad \text{Equation (3.2)}$$

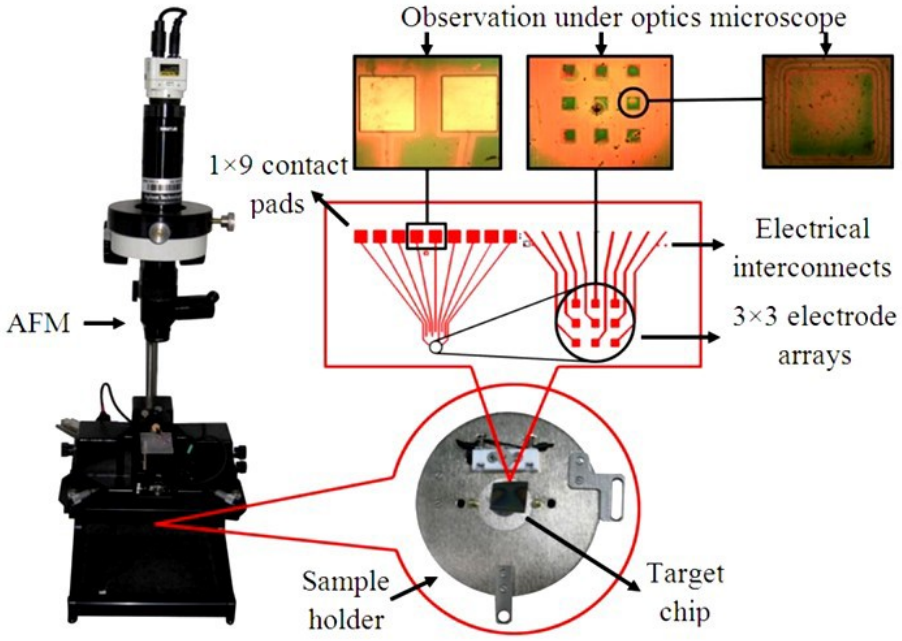

Figure 3.1. AFM-based experimental setup showing the sample holder and chips for scanning and characterization

3.3 Scanning and Measurement

Initially a 5 µm × 5 µm area was scanned in order to get the basic locations of the patterned nanofibers. Once the patterned nanofibers were recognized, then the image was zoomed in and rescanned with a 2 µm × 2 µm area to observe the nanofibers clearly and distinctly with a resolution of 100 nm. Figure 3.2(a) shows the 2D scan of a 5 µm × 5µm square area scanned after exposure to the environmental chamber. All the white dots in the image were the patterned VACNFs. It was obvious because they were arranged with a 1 µm gap and the pattern of the VACNFs was clearly seen in the image. After the identification of the nanofibers, the image was rescanned with a zoom into a much smaller area in order to clearly visualize the nanofibers. Figure 3.2(b) shows the 1.2 µm × 1.4µm zoom in of the 5 µm × 5µm square area. Patterned VACNFs were clearly seen, and at this point dimensions were calculated.

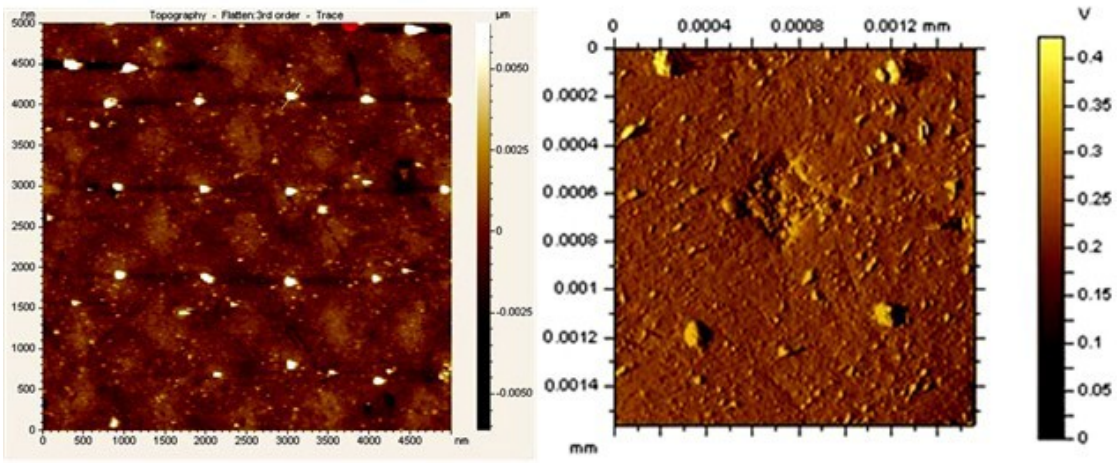

Figure 3.2. a) 2D cross section image of HF etched substrate from the AFM showing patterned CNFs. Scan size is 5µm × 5µm b) same image after the zoom in and rescan. Scan size is 1.2µm × 1.4µm

To obtain the dimensional data, a cross sectional line was drawn and the graph generated by drawing a cross sectional line was shown in Figure 3.3. While the distance between the two nodes was recorded as the diameter of the fiber, distance between the base line and the highest point in the curve was recorded as the height of the fiber.

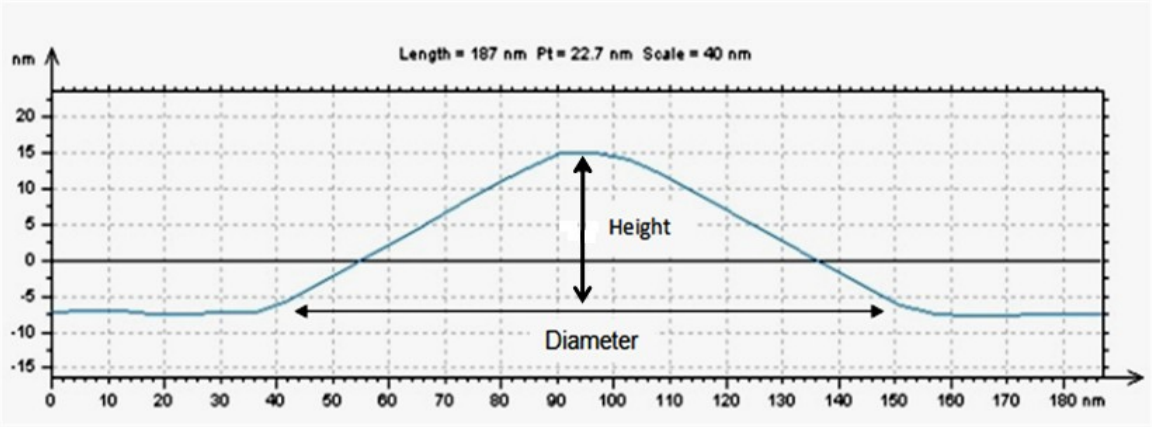

Figure 3.3. Cross section information for measurement based on line crossing (unetched)

For better analysis of the nanofibers, the 3D scan was converted to a perspective view 3D scan using software called the picoview. From the 3D perspective view, many details that were not clearly visualized from the 3D view were observed. For instance, the nanofiber tip shape from the side view was seen while it was not seen from the top view. Also, side view provides the information of how the fibers were oriented from the substrate and what height the nanofibers extended from the base. A sample of the 3D perspective images converted from the 3D scan was shown in Figure 3.4.

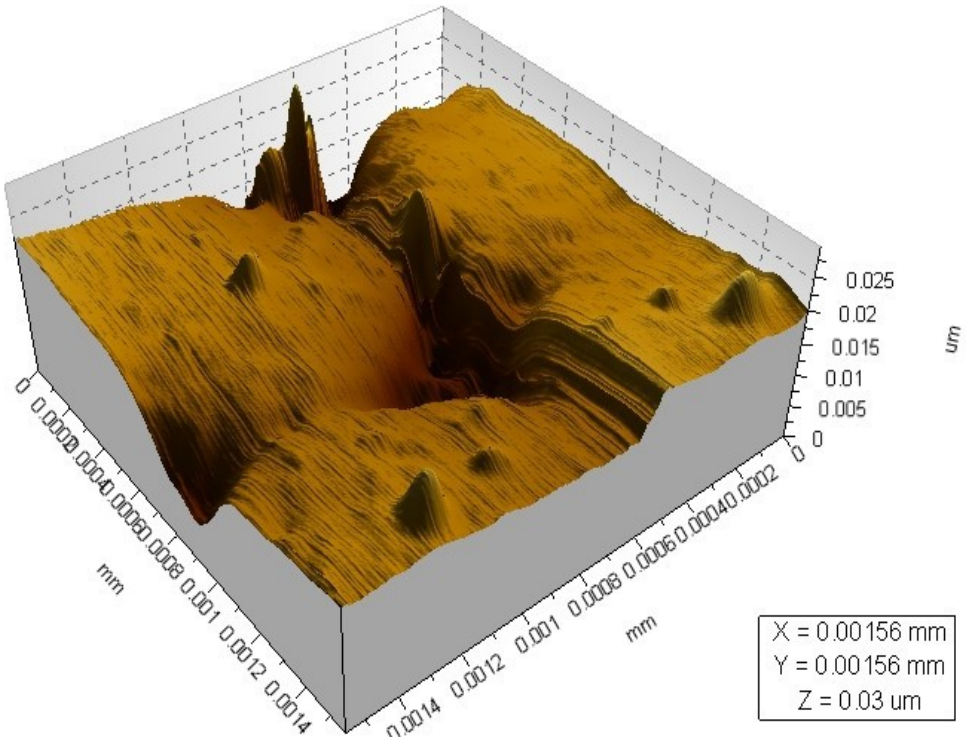

Figure 3.4. 3D Topography image generated from the 2D image. CNFs are clearly visible along with the cavities. Scan size is 1.2µm × 1.4µm.

From Figure 3.4, it was clearly observed that the fibers were spaced at even distances from one another, and that there was a cavity between them. This detail wasn't observed in the SEM scan done at NASA Ames research center. Also, it was seen that the tip of the fiber was pointed from the 3D perspective image while nothing was clearly visualized from the 3D image.

3.4 Results and Discussion

Ten measurements were recorded per each nanoelectrode array and on the whole 90 measurements were recorded for each temperature the substrate was subjected to. This accumulated a large set of data for 20 different temperatures (from $0^{o}C$ – $100^{o}C$ with a $5^{o}C$ increment, there will be 20 intervals). Thus, the average dimensional measurements were calculated for both unetched and HF etched nanoelectrode chips and were tabulated along with their standard deviations in Tables 3.1 and 3.2. Note that all the dimensional measurements were in nm and temperature was recorded in the centigrade scale. Since small scanner was used for the dimensional measurement, the dimensional values were measured to a resolution of 2 Å RMS. Substrates were cooled to room temperature ($23^{o}C$ for this experiment) after exposure to a particular temperature and dried until their relative humidity fell below 3%.

Table 3.1 Nanofiber Dimensions Average and Standard Deviation Data for Unetched Substrate at Different Temperatures

Temperature (^{o}C)	RH	Avg. Diameter (nm)	Diameter Std. dev	Avg. height (nm)	Height Std. dev.
0	51.8	152.8	22.8	8.4	2.2
5	41.5	156.6	24.1	8.9	2.4
10	24.5	141.3	6.4	9.4	1.9
15	21.3	151.5	15.2	9.5	4.5
20	17.0	154.2	16.1	10.1	2.6
25	10.0	148.2	12.5	7.9	1.5
30	10.0	128.6	7.7	7.2	1.6
35	10.0	151.3	9.9	7.4	1.4
40	10.0	161.5	9.1	5.5	1.1
45	10.0	158.1	16.5	8.7	1.5
50	10.0	171.7	17.5	6.9	1.5
55	10.0	140.1	14.7	5.7	1.2
60	10.0	164.6	14.8	4.7	1.3
65	10.0	142.9	12.6	6	1.5
70	10.0	156.0	18.9	8.8	1.9
75	10.0	157.4	27.3	8.5	2.3
80	10.0	171.2	34.8	7.6	1.6
85	10.0	164.1	27.4	8.3	1.8
90	10.0	173.1	36.5	8.7	2.8
95	10.0	169.3	29.1	8.4	2.7
100	10.0	181.7	14.1	7.5	1.8

Table 3.2 Nanofiber Dimensions Average and Standard Deviation Data for HF Etched Substrate at Different Temperatures

Temperature (^{o}C)	RH	Avg. Diameter (nm)	Diameter Std. dev	Avg. Height (nm)	Height Std. dev.
0	51.8	144.6	11.7	8.2	2.6
5	41.5	144.5	9.8	8.7	2.4
10	24.5	139.7	7.1	7.8	2.2
15	21.3	141.2	7.8	8.5	1.8
20	17.0	147.3	9.1	8.7	1.8
25	10.0	137.5	28.5	9.8	3.6
30	10.0	127.5	34.5	10.9	4.4
35	10.0	124.3	31.1	10	3.6
40	10.0	134.2	47.3	8.7	3.7
45	10.0	186.2	30.9	6.7	2.3
50	10.0	123.3	31.0	8.9	4.6
55	10.0	134.7	42.5	7.9	3.9
60	10.0	105.5	29.7	7.1	3.8
65	10.0	132.8	31.5	7.9	3.1
70	10.0	120.3	29.7	9.6	3.4
75	10.0	126.4	29.9	8.5	3.8
80	10.0	163.2	51.4	6.9	2.9
85	10.0	201.8	45.7	3.4	1.8
90	10.0	124.8	43.1	5.1	1.8
95	10.0	154.5	10.1	7.5	3.0
100	10.0	158.4	13.7	8.0	2.9

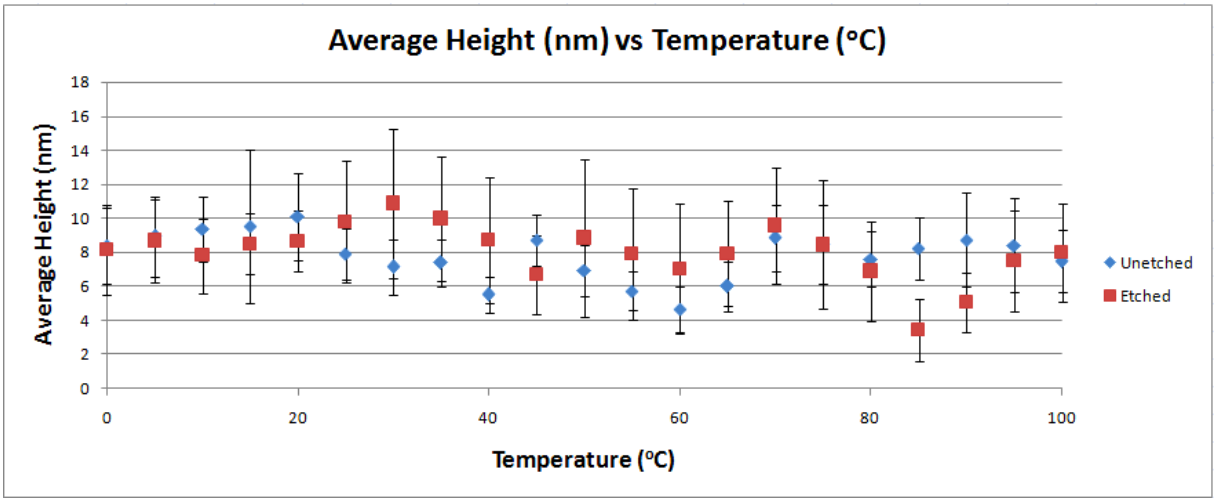

Figure 3.5 Graphs of the Average Height vs Temperature for both unetched and HF etched along with their standard deviations

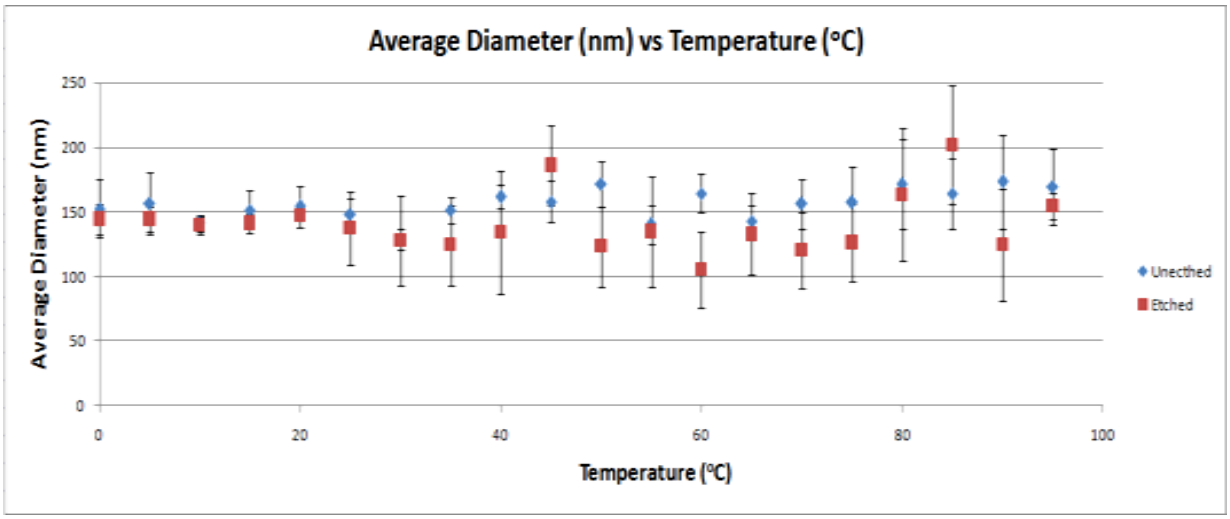

Figure 3.6. Graphs of the Average Diameter vs Temperature for both unetched and HF etched along with their standard deviations

Figures 3.5 and 3.6 were the graphical images generated from the average dimensional values vs temperatures shown in Tables 3.1 and 3.2. Figure 3.5 was the graph of the average height of unetched and HF etched substrates versus temperature. Graph was generated for the average diameter of unetched and HF etched substrates vs temperature as shown in Figure 3.6.

Taking variance of Figures 3.5 and 3.6 into consideration, there was no detectable effect of temperature on the dimensions of nanofibers in the ambient temperature range.

Prior researches on the carbon nanotubes have proven that the electrical conductivity of the nanotubes was inversely dependent on the length of the nanotube [66]. Assuming this result was applicable to carbon nanofibers, the conductivity of the nanofibers remains unchanged in the ambient temperature range.

3.5 Statistical Analysis

For experiments like these with high data acquisition, statistical analysis is of pivotal importance. In statistics, a confidence interval (CI) is an interval estimate of the overall population. It would help to define the population more accurately by assigning them a range which includes the mean of the population. This, in general, is calculated based on the mean and standard deviation of the population. The range varies based on the percent of the population that should be included. In general, for a data of 90 measurements, 95% population inclusion will be a very good estimate of confidence. Hence, we calculated the confidence interval for 95% population and Equation (3.2) shows us the method of calculating the confidence intervals (CI).

$$CI = \left[X - Z \times \frac{\sigma}{\sqrt{N}}, X + Z \times \frac{\sigma}{\sqrt{N}} \right] \qquad \text{Equation (3.2)}$$

Where, X is the mean value of the samples; Z, the critical value, is equal to 1.96 in a 95% *CI*; σ is the standard deviation and N is the number of the samples which is equal to 90 in this case. Detailed confidence intervals for each temperature were given in Tables 3.3 and 3.4. A sample calculation was shown below. For instance at a temperature of 0^{o}C, for unetched substrate, the average diameter was 152.8 nm while the average height was 8.39 nm, and their

standard deviations were 22.8 nm and 2.23 nm respectively. Now using the Z-value of 1.96, confidence intervals were calculated substituting the values in Equation (3.2). Thus the confidence interval was {152.8 − 1.96 × 22.8/ 90^0.5, 152.8 + 1.96 × 22.8/ 90^0.5} and the confidence interval was attained for the inclusion of 95% population.

From the confidence interval data, it was clearly evident that all the data acquired for a particular temperature fell within the range of 15 nm for diameter and 2 nm for height, indicating the accuracy of the microscope. As the average was comprised of 90 measurements, it was sure that the values were precise and accurate to a hundredth of a nanometer.

Table 3.3 Confidence Intervals of Diameter and Height at Different Temperatures for Unetched Substrate

Temperature (^{o}C)	Diameter CI		Height CI	
	LB	UB	LB	UB
0	148.1	157.5	7.9	8.9
5	151.7	161.6	8.5	9.4
10	140.0	142.6	9.0	9.8
15	148.4	154.6	8.6	10.5
20	150.9	157.5	9.6	10.6
25	145.6	150.7	7.6	8.2
30	127.0	130.2	6.8	7.5
35	149.2	153.3	7.1	7.7
40	159.6	163.3	5.3	5.7
45	154.7	161.5	8.4	9.0
50	168.0	175.3	6.6	7.3
55	137.0	143.1	5.5	6.0
60	161.5	167.6	4.4	5.0
65	140.3	145.5	5.7	6.3
70	152.1	159.9	8.4	9.2
75	151.8	163.0	8.0	8.9
80	163.9	178.4	7.3	7.9
85	158.5	169.8	7.9	8.6
90	165.6	180.7	8.2	9.3
95	163.3	175.3	7.9	9.0
100	178.8	184.6	7.1	7.9

CI indicates confidence Interval. LB, UB indicates Lower and Upper Boundaries respectively. All dimensions are in nm.

Table 3.4 Confidence Intervals of Diameter and Height at Different Temperatures for HF Etched Substrate

Temperature (^oC)	Diameter CI		Height CI	
	LB	UB	LB	UB
0	142.2	147.0	7.6	8.7
5	142.5	146.5	8.2	9.2
10	138.2	141.2	7.4	8.3
15	139.6	142.8	8.1	8.9
20	145.4	149.2	8.3	9.0
25	131.6	143.4	9.1	10.6
30	120.4	134.6	10.0	11.8
35	117.9	130.7	9.2	10.7
40	124.4	144.0	8.0	9.5
45	179.8	192.5	6.2	7.2
50	116.9	129.7	7.9	9.8
55	126.0	143.5	7.1	8.7
60	99.3	111.6	6.3	7.8
65	126.3	139.3	7.3	8.6
70	114.2	126.5	8.9	10.3
75	120.2	132.6	7.7	9.2
80	152.6	173.8	6.3	7.5
85	192.4	211.2	3.1	3.8
90	115.9	133.7	4.7	5.4
95	152.4	156.6	6.9	8.1
100	155.6	161.2	7.4	8.6

CI indicates confidence Interval. LB, UB indicates Lower and Upper Boundaries respectively. All dimensions are in nm.

Looking at the confidence interval data furnished in Table 3.3 and Table 3.4, it was concluded that the range was within 15 nm for diameter and within 2 nm for height for both unetched and etched cases.

3.6 Conclusion

The temperature effect on the VACNFs was successfully characterized using AFM in the ambient temperature zone. From the current experimental results it was concluded that temperature did not have any effect on the unetched and the etched carbon nanofibers dimensions in the ambient temperature range.

4. EXTREME ENVIRONMENTAL BEHAVIOR OF CARBON NANOFIBERS

4.1 Introduction

NASA, in a report submitted on the reasons for failure of its outer space missions [58], concluded that extreme environments of temperature and pressure, and cosmic radiations are the primary sources for the damage of the instruments, and thus, reason for the failure of the missions. Sensors that are attached to the rovers and other space exploration objects have more threats as they need to do the sampling of unknown environments. Payload weight is one of the most critical factors in the space missions. Figure 4.1 contains a table which shows the critical design factors that need to be considered for several of the ongoing / futuristic missions planned by NASA. As shown in the table in Figure 4.1, almost every mission is a failure because of extreme temperatures and/or radiation. Thus, it is of prime importance that we understand the behavior of the materials in those environments before setting up for an actual mission. Sensors are the most vulnerable of all as they need to withstand radiation, extreme environments and need to interact with unknown chemicals. So it's a real challenge for researchers to find a solution to these problems.

A statement retrieved from NASA Ames Research Center webpage says[57] *"Our current sensor development results have proved that the carbon nanotube sensors can offer very high sensitivity for NO_2 , ammonia, methane, acetone, benzene and toluene detection, with detection limits in the lower ppm to ppb level and response time in seconds to minutes. Each sensor draws the power in micro-watts to milli-watts. The size of the detector is designed to be 5 ´ × 5 ´ × 1' for 32 sensing elements detection system. The weight of this detector will be less than 2 kg."*

Thus, carbon nanofibers offer a viable solution provided they survive the extreme outer space environments, and chips of carbon nanofibers are already hooked up to the international space station (ISS) and are being tested to determine if they can survive the radiation and function properly.

Mission stage		Space	Entry		In situ					
Target	**Proposed Mission Architecture**	Radiation	Heat flux at atm. entry	Deceleration	High Pressure	Low temperatures	High temperatures	Thermal cycling	Chemical corrosion	Physical corrosion
High temperatures and high pressures										
Venus Surface	Air mobility, lander or rover		✓	✓	✓		✓		✓	✓
Saturn	Atmospheric entry probes		✓	✓			✓			
Jupiter	Atmospheric deep entry probes		✓	✓	✓		✓			
Low temperatures										
Lunar polar regions	Lander / rover					✓		✓		
Comet nucleus	Sample return		✓			✓				
Titan surface	Balloon, aerobot, lander / rover		✓	✓		✓				
Low temperatures and high radiation										
Europa orbit	Orbiter	✓				✓				
Europa surface	Orbiter w/ lander	✓				✓				
Thermal cycling										
Mars	Lander/rover					✓		✓		✓
Moon	Lander/river					✓		✓		✓
Mercury	Lander					✓		✓		

Figure 4.1. Table showing the design considerations for various space missions. Retrieved from the NASA report for failure of outer space missions [58]

The effect of extreme environments and the corrosive substances on carbon nanofibers was studied and detailed in the following sections.

Nanoindentation technique was used to measure the Young's modulus, hardness and elastic modulus of the material. Indentation is a long known technique that has been effectively used to measure mechanical properties of material. Nanoindentation was successfully used to study the mechanical properties like Young's modulus, hardness and elastic modulud of materials [70-74] and proved to be a very reliable method to study the mechanical properties. In a typical indentation process, a hard tip with known mechanical properties (generally made of diamond) is pressed against a material with unknown mechanical properties. A load displacement curve is then plotted from the obtained data, and this gives the Young's modulus of material. Thus, the use of Nanoindentation for measurement of Young's modulus is justified.

4.2 Effect of Extreme Temperatures on VACNFs

4.2.1 Introduction

As mentioned in the previous section, materials may behave much differently under extreme environments. Especially when the body is subjected to low temperatures, it tends to either acquire plastic nature and deform or become brittle and break easily. If our planetary system is observed, most of the planets, and their satellites, are engulfed by extreme low environments. It is thus required to understand the materials properties in those environments.

Carbon nanofibers have a huge potential in the realm of sensors. There is a high possibility that sensors made of carbon nanofibers will be used in the space because of their extraordinary properties of detection down to a single molecule, and they take very little confined space and mass. Hence their behavior in the extreme environmental conditions was studied in this work.

4.2.2 Experimental Setup

The fabricated chips were subjected to extreme environments in a controlled environmental chamber. For this purpose, a Microclimate Environmental Chamber (Manufactured by Cincinnati Sub Zero model No. MCBH 1.3) with an error of ±0.5% in the range of -70^{o}C – 100^{o}C was used. In this method, the environmental chamber was set to a fixed temperature. After the attainment of the specified temperature, the substrate with nanofibers was placed in the environmental chamber for 30 minutes. Then, the substrate was immediately transferred to an AFM for measurement of dimensions and mechanical properties. The overall measurement process took 5 minutes and a change of 3^{o}C was the predicted temperature change (according to the AFM specification) for this time period.

4.2.3 Atomic Force Microscopy (AFM)

The samples were analyzed for dimensional changes and mechanical fatigue using an AFM (Agilent 5500 SPM, Agilent Technologies, Inc., Santa Clara, CA, US). A Scanning Electron Microscope (SEM) was also employed to further characterize the nanofibers.

4.2.3.1 Scanning and Measurement

An Atomic Force Microscope (AFM) was used for accurate measurement of fiber dimensions after the treatment in the environmental chamber. Dimensional measurement was carried out in Acoustic AC (Tapping) mode with a Tap190DLC (BudgetSensors, Innovative Solutions Bulgaria Ltd.) probe [75] which had a resonant frequency of 190 KHz and a force constant of 48 N/m. For an applied setpoint voltage of 0.4 V and the sensitivity of 66.5 nm/V, the applied tip force (F_{tip}) was calculated as 1.3 µN. In atomic force microscopy, a large area of 5 µm × 5 µm was scanned initially in order to locate the nanofibers. As mentioned in the fabrication methodology, the nanofibers were grown on patterned Ni dots with a spacing of 1

μm. Scan images generated from the AFM and the SEM were shown in Figure 4.2. Standing carbon nanofibers at spacing of 1 μm were clearly seen in the Figure 4.2. Once the nanofibers were identified, the substrate was rescanned to shrink the area to 2 μm × 2 μm in order to more accurately measure the nanofiber dimensions.

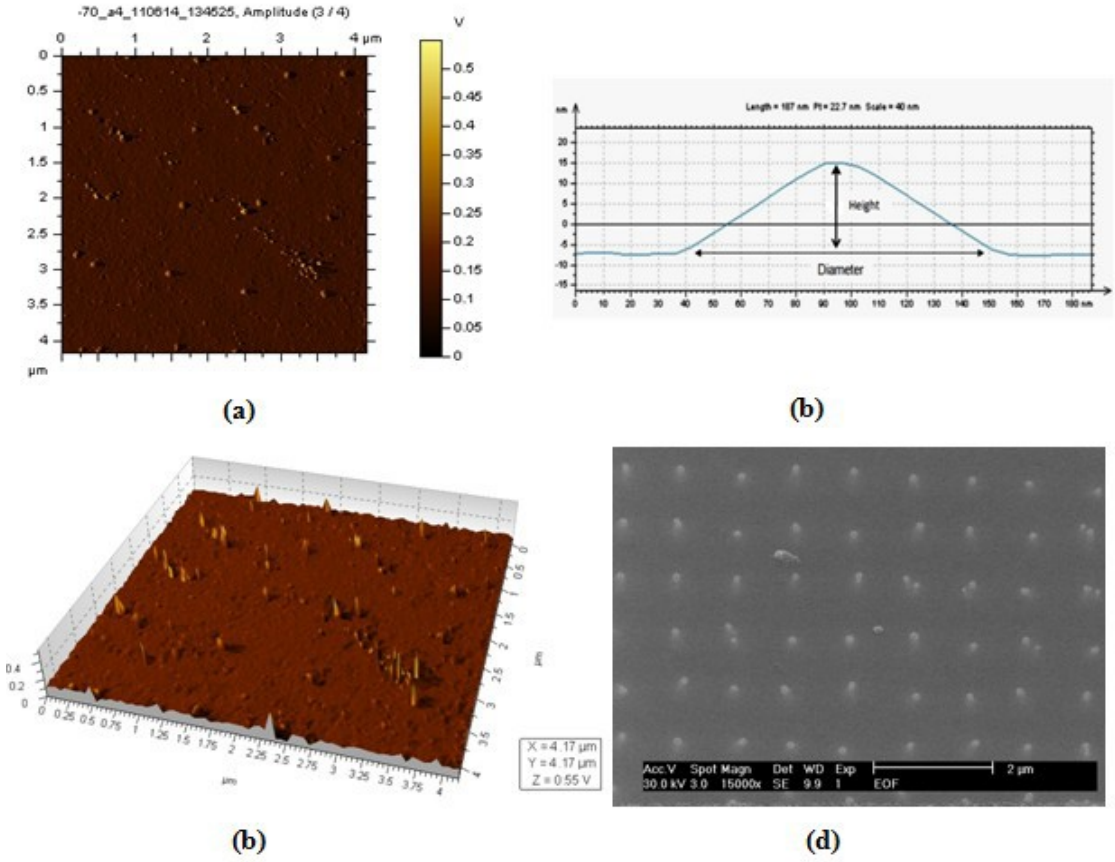

Figure 4.2. The AFM and the SEM scan images of nanofibers. a) 2D scan image of the nanofibers generated by the AFM. Scan size is 5 μm × 5 μm. b) Graph obtained by drawing a traversal across the nanofiber c) 3D scan image of the nanofibers generated by the AFM Scan size is 5 μm × 5 μm d) A SEM scan image of the nanofibers showing the evenly spaced CNFs

At this point, an arbitrary cross-section line was drawn over one nanofiber in the scanned image. This generated a 2D graph, as shown in Figure 4.2(b), of the nanofiber, from which the fiber dimensions were obtained. As shown in the Figure 4.2(b), the distance between the bases of

the curve was interpreted as the diameter of the nanofiber, while the distance between the base and apex was interpreted as the height of the nanofiber. In order to understand further, the 2D image was converted to the 3D perspective image using the AFM tool PicoImage. Figure 4.2(c) shows a 3D image obtained from the 2D scan image of Figure 4.2(a). From the 3D image, evenly spaced, vertically aligned and free standing carbon nanofibers were clearly seen. From the 3D image, the shape of the nanofibers was clearly seen from all directions, and thus, the temperature effect on the shape of the nanofiber was observed. Figure 4.2(d) shows the SEM image of the nanofibers scanned using a Philips SEM at 30 KeV. Nanofibers were clearly seen as the white dots in the black background. Twenty measurements of nanofiber dimensions were taken after each exposure to the environmental chamber.

4.2.3.2 Nanoindentation

In order to estimate the Young's Modulus, an important mechanical property of carbon nanofibers (CNFs), the atomic force microscope was used to scan the vertically aligned carbon nanofibers (VACNFs). After locating VACNFs by scanning a 5 µm × 5 µm area on the nanoelectrode arrays under Acoustic AC Mode, the AFM was utilized to perform nanoindentation on the located VACNFs. The AFM probe [71] was made of silicon with a 15 nm-thick diamond-like-carbon coating and had an approximate conical shape, which had a half cone angle (α) of about 25 degrees depicted in Figure 4.3. Its force constant and resonant frequency was 48 N/m and 190 kHz respectively. The tip diameter was less than 20 nm, while the diameter of the fibers ranges from 110 nm to 250 nm. Thus, the Sneddon model [76] (cone-on-flat) as shown in Figure 4.3(b) was employed to approximate this indentation process assuming the diamond-like-carbon coated probe was a rigid indenter. The relationship between

the indentation force ($F_{Sneddon}$), indentation distance (), Poisson's Ratio () and Young's Modulus (E_{sample}) of the fibers (sample) is described in Equation (4.1) [72] as follows:

$$F_{sneddon} = \frac{2}{\pi} \frac{E_{sample}}{1-\nu_{sample}^{2}} \delta^{2} Cot(\alpha) \qquad \text{Equation (4.1)}$$

From the AFM based nanoindentation, an amplitude displacement graph was obtained and knowing the sensitivity and force constant values allowed the force applied ($F_{Sneddon}$) and indented distance (δ) to be calculated. Then, the relation of $F_{Sneddon}$ to δ^2 was further derived and plotted. The slope ($F_{Sneddon}/\delta^2$) was approximated using a linear curve fit. The Poisson's Ratio, υ of the carbon nanofibers was assumed to be 0.06, which is Poisson's Ratio of Carbon Nanotubes [77]. Therefore, the only unknown variable left in the Equation (4.1) was E_{sample}, and it was computed easily by algebraic manipulation. Equation (4.2) describes the relationship between the piezo scanner movement in the z-axis (Δz), the cantilever deflection (Δd) and δ, and Equation (4.3) shows how to determine the indentation force, where k_c is the force constant of the cantilever.

$$\Delta z = \Delta d + \delta \qquad \text{Equation (4.2)}$$

$$F = k_c \times \Delta d \qquad \text{Equation (4.3)}$$

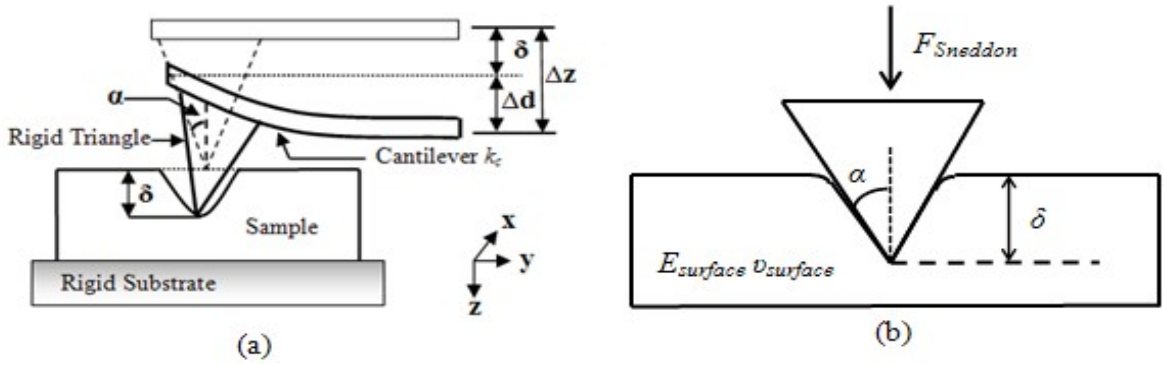

Figure 4.3. Schematic for AFM-based nanoindentation: (a) illustration of z-axis movement, cantilever deflection and indentation distance; (b) the Sneddon model.

4.2.4 Results

4.2.4.1 Dimensional measurement data analysis

Figure 4.4 shows the 3D images of VACNFs generated from PicoImage after being exposed to different sub-zero temperatures. As seen from the 3D images, there was change to the shape of the nanofibers before and after treatment. For accuracy, 20 measurements were recorded and averaged. Table 4.1 shows the average and the standard deviation of nanofibers after exposure to the extreme environments. From the Table 4.1, it was clear that most of the nanofibers responded to the temperature changes. In most cases, the nanofiber dimensions decreased compared to that of room temperature (23^{o}C). Furthermore, it was concluded that there was an initial contraction of the nanofiber, and the dimension of the nanofiber remained constant at all the sub zero temperatures compared to the dimensions at room temperature.

Table 4.1 Average Diameter and Height of Nanofibers after Exposure to Temperatures

Temperature (°C)	Average Height (nm)	Average Diameter (nm)	Standard Deviation of Height (nm)	Standard Deviation of Diameter (nm)
Room	8.9	254.0	1.3	36.4
-20	5.3	189.5	0.9	27.5
-30	6.7	136.8	2.4	21.8
-40	5.4	112.8	1.3	15.4
-50	6.5	118.6	2.3	22.3
-60	6.0	173.2	1.2	17.0
-70	6.6	120.5	1.6	20.0

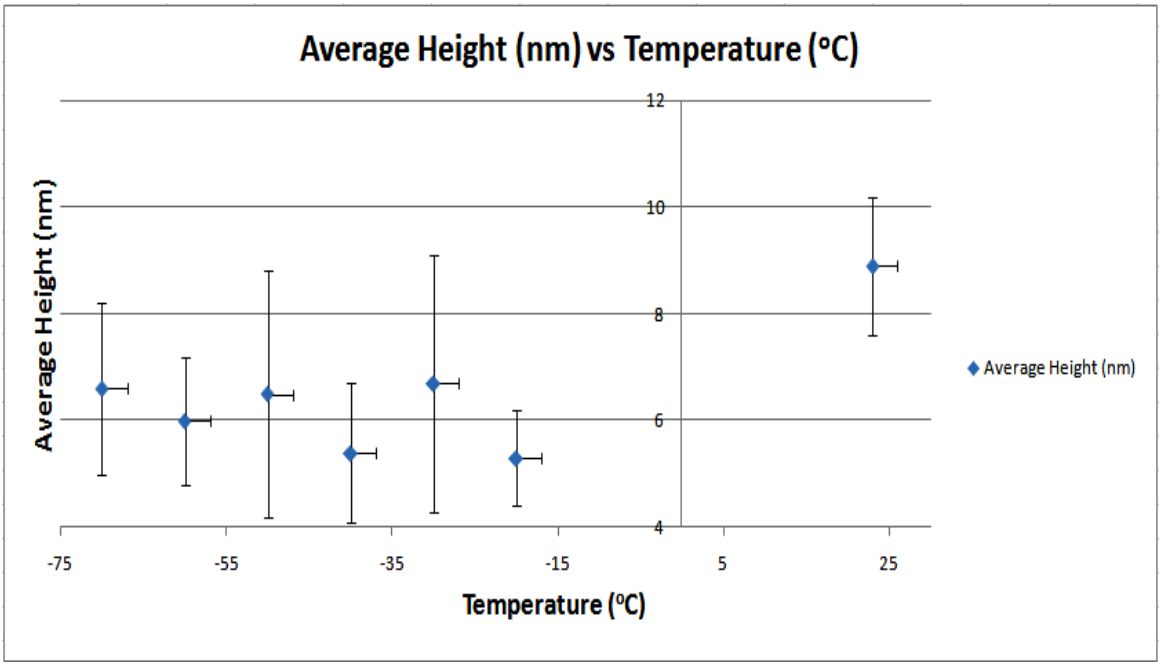

Figure 4.4 Average Height vs Temperature for subzero temperartures

Average height versus temperature from Table 4.1 was plotted as graph in Figure 4.4. Change in nanofiber height was clearly observed from the graph. It is a well known fact that most materials at the macroscopic scale contract when cooled. Even though this very fundamental phenomenon is supported by the nanofibers compared to that at room temperature,

they became resistant to dimensional changes at lower temperatures contradictory to what was predicted. It is because the carbon nanofibers reached the configuration of minimal lattice distance separation, wherein other forces like the electrostatic repulsion became a dominant force and oppose further contraction of the nanofibers.

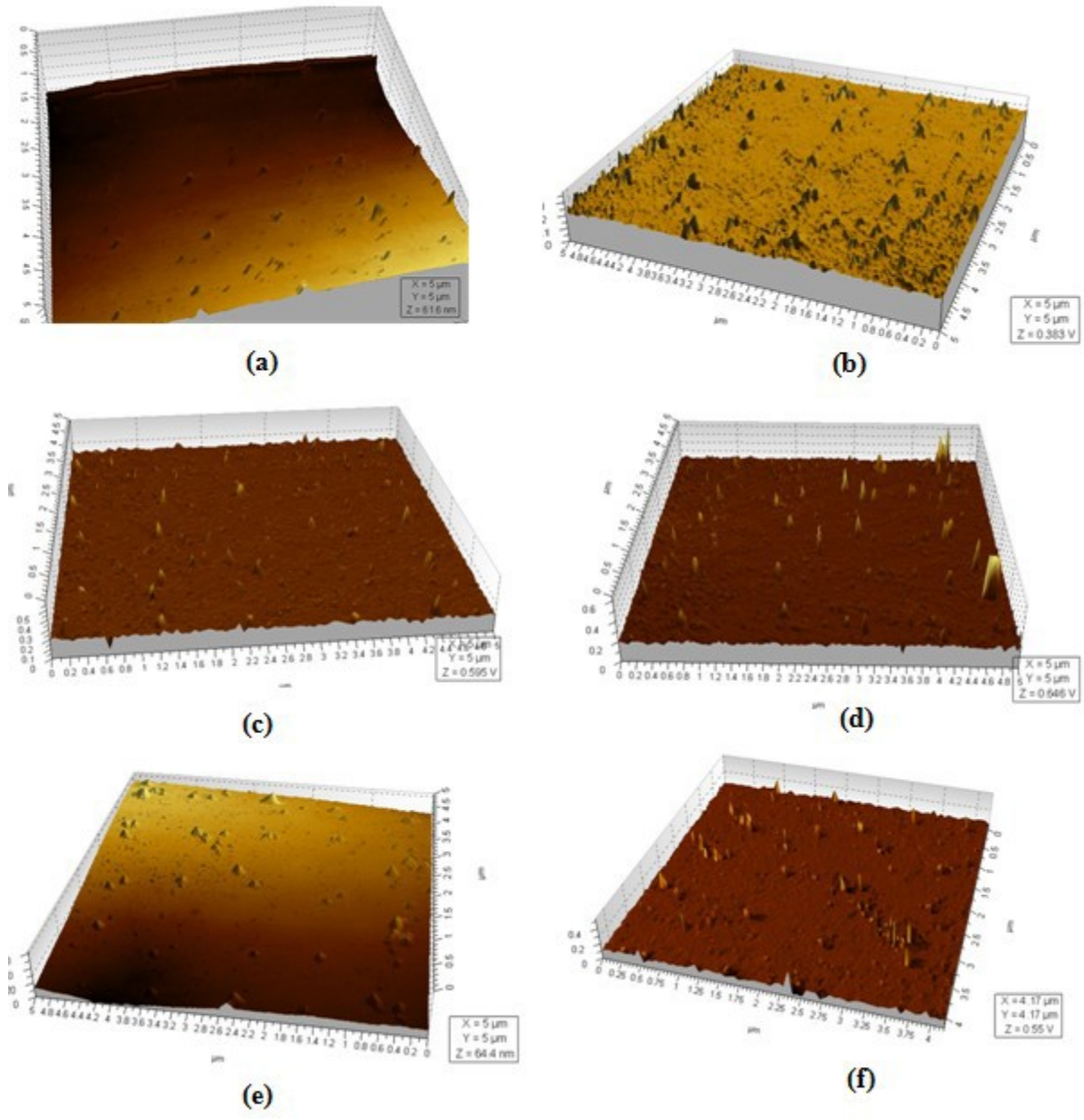

Figure 4.5. A through F: 3 D scan images generated from the AFM based picoImage software after exposure to different temperatures. a) -20^{o}C b) -30^{o}C c) -40^{o}C d) -50^{o}C e) -60^{o}C f) -70^{o}C. Scan sizes are 5 µm × 5 µm

4.2.4.2 Nanoindentation Analysis

The nanoelectrode arrays were scanned to locate VACNFs, and Figure 4.5(f) shows the VACNFs that were treated in the environmental chamber at -70ºC for 30 minutes. The tip was then positioned on the top of one of the located fibers followed by a sweep of amplitude versus distance in a vertical direction. Thus, the raw data of indenting a nanofiber was obtained as shown in Figure 4.6 (a), where "Amplitude" describes Δd and "Z" represents Δz. In order to convert the amplitude in V into the cantilever deflection in nanometer (nm), calibration of sensitivity was necessary. Before scanning the nanoelectrode arrays, the same tip was used to indent a mica disc surface 5 times. During this indentation period, the mica surface was assumed to be rigid, which indicated δ=0. Hence, the deflection of the cantilever Δd equals the vertical displacement Δz, which was controlled by the user when an indentation sweep was engaged.

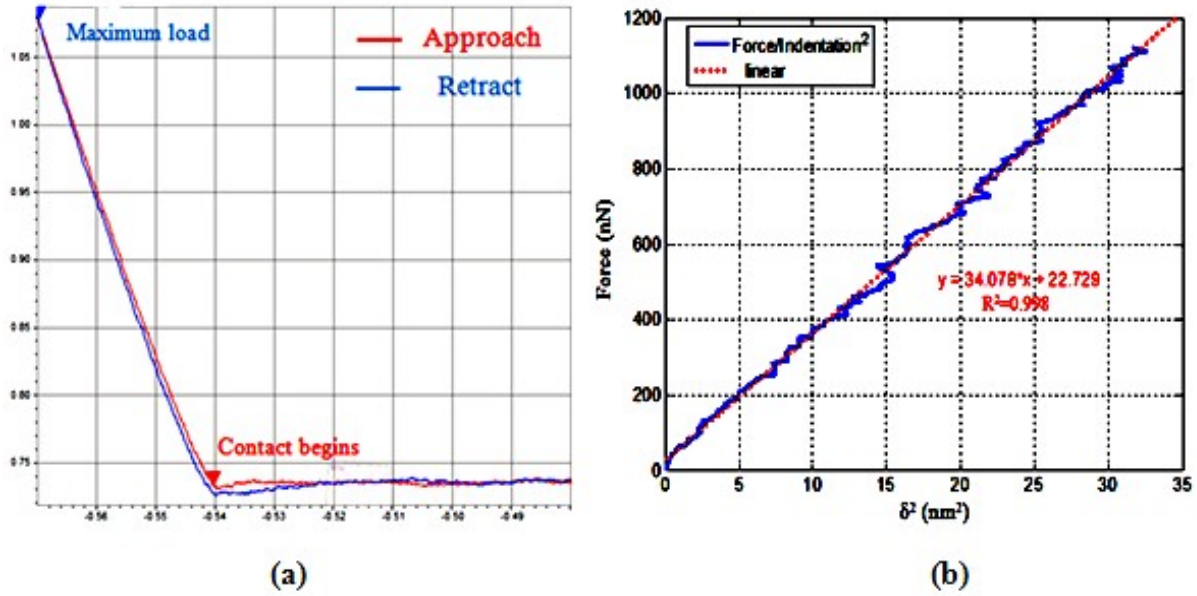

Figure 4.6. a) Amplitude Displacement curve obtained by Nanoindentation. b) Force ($F_{sneddon}$) versus Indentation (δ^2) generated from the raw data of Nanoindentation.

Therefore, the sensitivity was obtained, and its mean value was calculated to be 68.5 nm/V with a standard deviation of 0.55 nm/V. With this sensitivity, the relation between the force and the indentation distance was obtained. Furthermore, the slope of force versus δ^2 was approximated by a linear fit as shown in Figure 4.6(b). The linear fit provided the slope approximation, which is 34.078 nN/nm^2. Finally, this slope was substituted in Equation (4.1) to compute the value of the Young's Modulus, E_{VACNF} = 23.9628 GPa. Table 4.2 shows the results of E_{VACNFs} at different temperature treatments.

Table 4.2 Young's Modulus Calculated From the Nanoindentation Data for Three Different Fibers after the Exposure to Extreme Environments

Temperature (^{o}C)	Sample 1	Sample 2	Sample 3
Room	511.8	1240.4	1010.7
-20 + 3	44.0	124.8	50.8
-30 + 3	70.4	64.4	80.9
-40 + 3	59.2	50.9	40.5
-50 + 3	37.7	34.2	55.1
-60 + 3	41.0	40.7	30.2
-70+ 3	23.5	20.8	26.9

All Dimensions are in GPa

4.2.5 Discussion

4.2.5.1 Dimensional Measurement

From the dimensional results, it was noted that the dimensions of the CNFs were affected upto 50% by the changes in temperatures from -70^{o}C – 100^{o}C. This was critically important because of the fact that most materials properties at nanoscale depend on the dimensions as well. The fabrication methodology involved the carbon nanofiber side wall passivation to enhance tip

binding and thus sensing. Thus this project particular interest lies in changes to the height of the nanofiber compared to the diameter as the side walls of the nanofiber were passivated by the silicon dioxide (SiO_2), and it led to much more complex material behavior. From the dimensional results, it was observed that the nanofiber height decreased with the temperature when compared with the original room temperature. However, in the subzero range, any height change could not be detected due to the large scatter in the data.

4.2.5.2 Mechanical Properties Measurement:

Mechanical properties of the nanofibers exposed to subzero environments were studied in detail. Young's modulus of the nanofibers was calculated at different temperatures. A Young's modulus of 920.0 ± 372.5 GPa was calculated for nanofibers at room temperature. These values are in accordance with the Multi Walled Carbon Nanotubes (MWCNTs) Young's modulus of ~ 1 TPa calculated from the prior experimental works [78, 79]. However, the Young's modulus of the VACNFs fell twenty fold as the substrate was exposed to temperatures less than room temperature. It was observed from the Table 4.2 that the Young's modulus of the fiber almost reduced by 20 fold at subzero temperature range. Positioning of the cantilever on the carbon nanofiber was of pivotal importance in the experiement. Any bend in the nanofiber from edge placement of the probe led to a lower value of Young's moduls. Therefore, the highest value of the three samples was considered as the most appropriate value for Young's modulus of the carbon nanofibers corresponding to that temperature. This assumption was completely justified by the measurements at the room temperature. While the highest value of Young's modulus obtained at room temperature was 1240 GPa, the lowest value was 511 GPa. Comparing with theoretical values of Young's modulus at room temperature i.e., ~ 1000 GPa, the explination

above was seen to have merit. Thus a plot of highest obtained Young's modulus value for each temperature was plotted against temperature as shown in Figure 4.7.

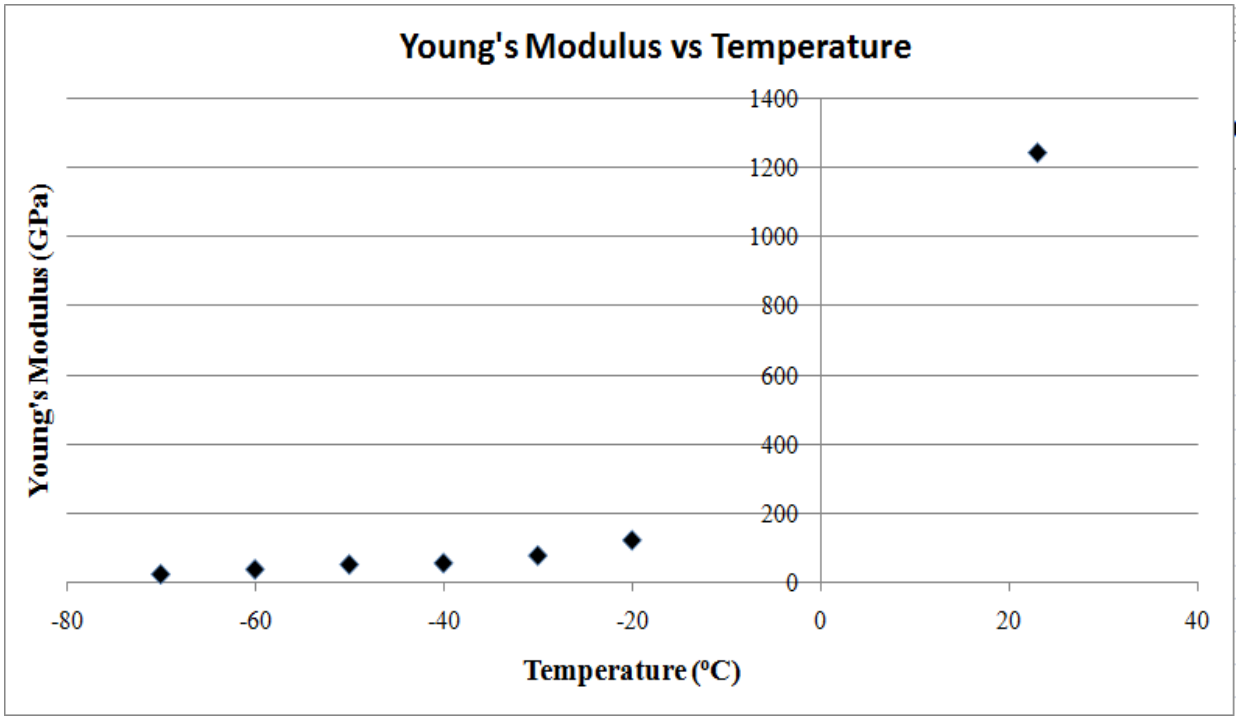

Figure 4.7. Young's Modulus vs Temperature

4.2.6 Conclusion

From the current experimental results it was inferred that the VACNFs lose their stiffness in an exponential manner with respect to decrease in temperatures. It was also observed that there was a decrease in height of the nanofibers compared to the room temperature while the height of the nanofiber remained constant in the sub zero range. For the first time, AFM based Nanoindentation was used for the calculation of the mechanical properties of the nanofibers and the Sneddon model was used for obtaining the Young's modulus of the nanofibers.

4.3. Effect of Acids on VACNFs

4.3.1 Introduction

Corrosive substances are the substances which can chemically damage the surface of other materials in an irreversible manner. Due to this damage, many times the other materials lose their functional capabilities; like in nanofibers case, the sensor would lose their sensitivity. It was of high possibility that the sensor might interact with corrosive substances in space application, when it is exposed to an unknown sample. Strong acids are one category of the corrosive substances which are present almost everywhere and are a key of corrosive family substances. Thus, the effect of acids corrosion on the VACNFs was studied. The corrosion rate was taken as the measure of the effect of acids on the carbon nanofibers, and the corrosion rate is given by Equation (4.5).

$$\text{Corrosion Rate} = \frac{\text{Change in Height}}{\text{Time}} \qquad \text{Equation (4.5)}$$

As shown in the Equation (4.5), a corrosion rate was only measured for the height as the sidewalls were protected by the thick layer of Silicon Dioxide. Thus, a height corrosion rate was the only measurement considered.

4.3.2. Experimental Setup

A standard Wet bench technique was used to treat the VACNF chips in acids. All the acids except the HF were taken in 5 N concentrations, the chip was allowed to react with the acids for 5 minutes, and then the chip was measured for the changes in the dimensions. Since the sidewalls of the carbon nanofiber were passivated, the acid cannot corrode the CNF until it completely corrodes the Silicon Dioxide (SiO_2) layer. As the SiO_2 layer was a 3 µm ± 0.8%

thick, it offered a greater protection to the sidewalls. Hence only the corrosivity of the material for the change in height was measured. After the treatment of the VACNF chips, the chips were cleaned and rinsed in distilled water, dried using air, and then kept in the dry box until their Relative Humidity (RH) value fell below 3%. The samples were then measured using the AFM.

4.3.3. Scanning and Measurement

An AFM was used to scan the dimensions of the acid treated nanofibers. Figure 4.8 shows the AFM setup used to measure the changes in the dimensions of the fibers after acid treatment. As shown in the Figure 4.7, the acid treated, cleaned and dried chip was then loaded on to the sample holder and measured using AFM. A small scanner with Tap 190Al-G probe of 190 KHz frequency and a 48 N/m force constant was used in tapping mode i.e., intermittent contact mode to scan the fibers. This way it was made sure that the AFM didn't damage any surface integrity or didn't cause any scratches on the surface. A tip force of 1.3 µN was applied using a setpoint voltage of 0.4 V. A scan area of 5 µm × 5 µm was scanned initially to locate the nanofibers. Once the nanofibers were located, the scan area was zoomed in to get a better image and to obtain the nanofiber dimensional data. Dimensional data was obtained from the graph that was created by drawing a traverse across the nanofiber. For statistical purposes, dimensions of 70 nanofibers were collected and analyzed.

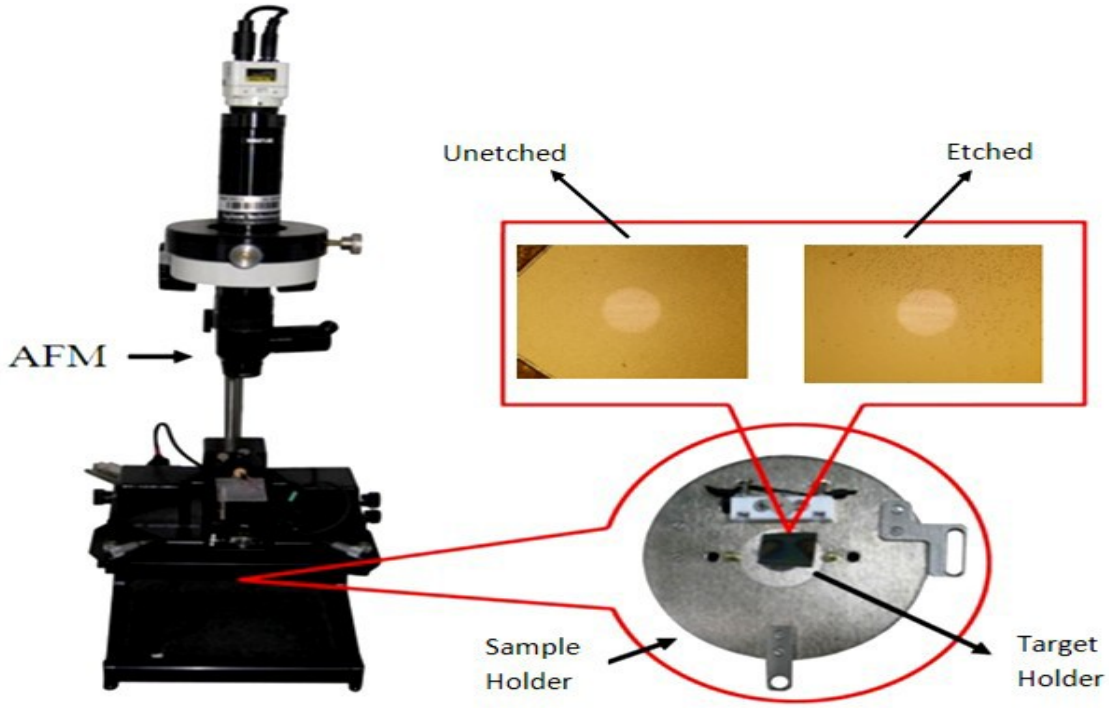

Figure 4.8. An AFM-based experimental setup showing the sample holder and chips for scanning and characterization

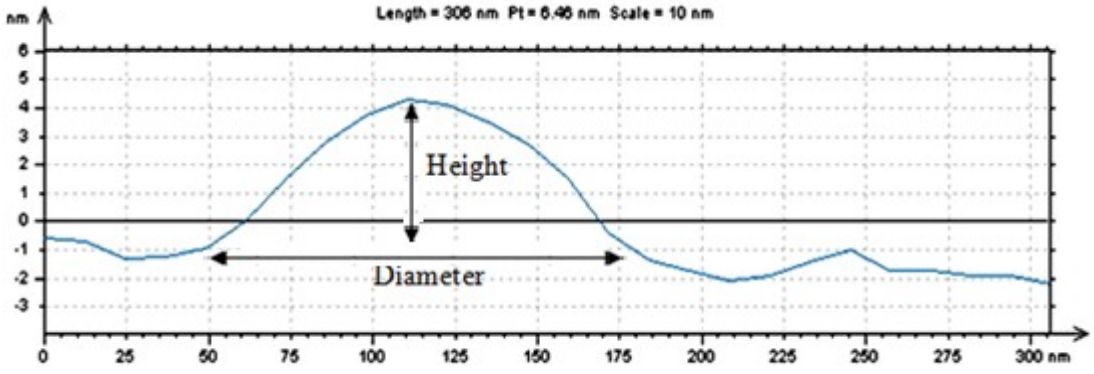

Figure 4.9. Graph obtained by drawing a line over the CNF using the AFM software

After the sample was loaded, AFM was used to scan the surfaces. After identifying the fibers, a line was drawn over the fiber and shown in the graph shown in Figure 4.9. The distance between the nodes indicated the diameter while the amplitude of the curve indicated the height of the nanofiber. Figure 4.10 shows the images of the 2D scans of the topographies of untreated to

different acid treated chips. An untreated surface is shown in Figure 4.10(a) while acetic acid (CH_3COOH) treated surface is shown in Figure 4.10(b), sulfuric acid (H_2SO_4) treated surface is shown in Figure 4.10(c) and hydrofluoric acid (HF) treated surface is shown in Figure 4.10(d).

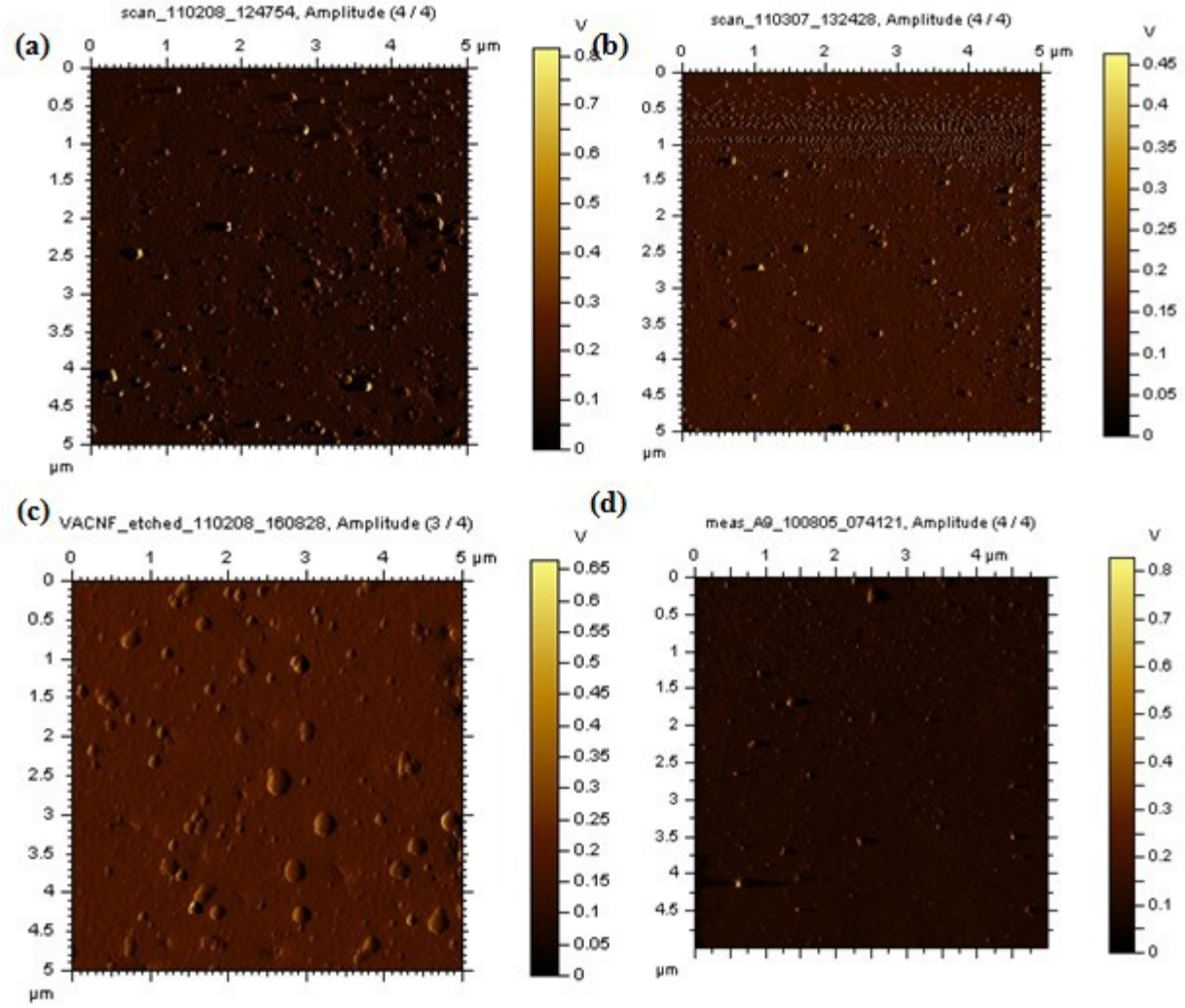

Figure 4.10. 2D AFM scan images before and after acid treatment a) Untreated, Scan size is 1.5 µm × 1.5 µm b) Acetic acid treated c) sulfuric acid treated and d) HF treated. Scan sizes are 5 µm × 5 µm

4.3.4 Results and Discussion

From Figure 4.10, it was clearly evident that different acids have corroded the surface of the substance differently. While the acetic acid treated CNFs were more pointed and thin,

sulfuric acid treated CNFs were more bulged and short. HF treated chips became completely rough as the HF is known to etch the Silicon Dioxide layer. Thus the HF treated image displayed cavities and there was a vast reduction in the number of fibers per unit area compared to the untreated surface. In order to have a better view and understanding the 2D images were converted to 3D using the AFM simulation software known as the PicoImage. Figure 4.11 shows the 3D images that were generated from the PicoImage. Many of the unseen results were seen by converting the image to 3D. As seen from the Figure 4.11, while the sulfuric acid resulted in a fiber with blunt shape, both acetic acid and hydrochloric acid resulted in a fiber with sharp edge.

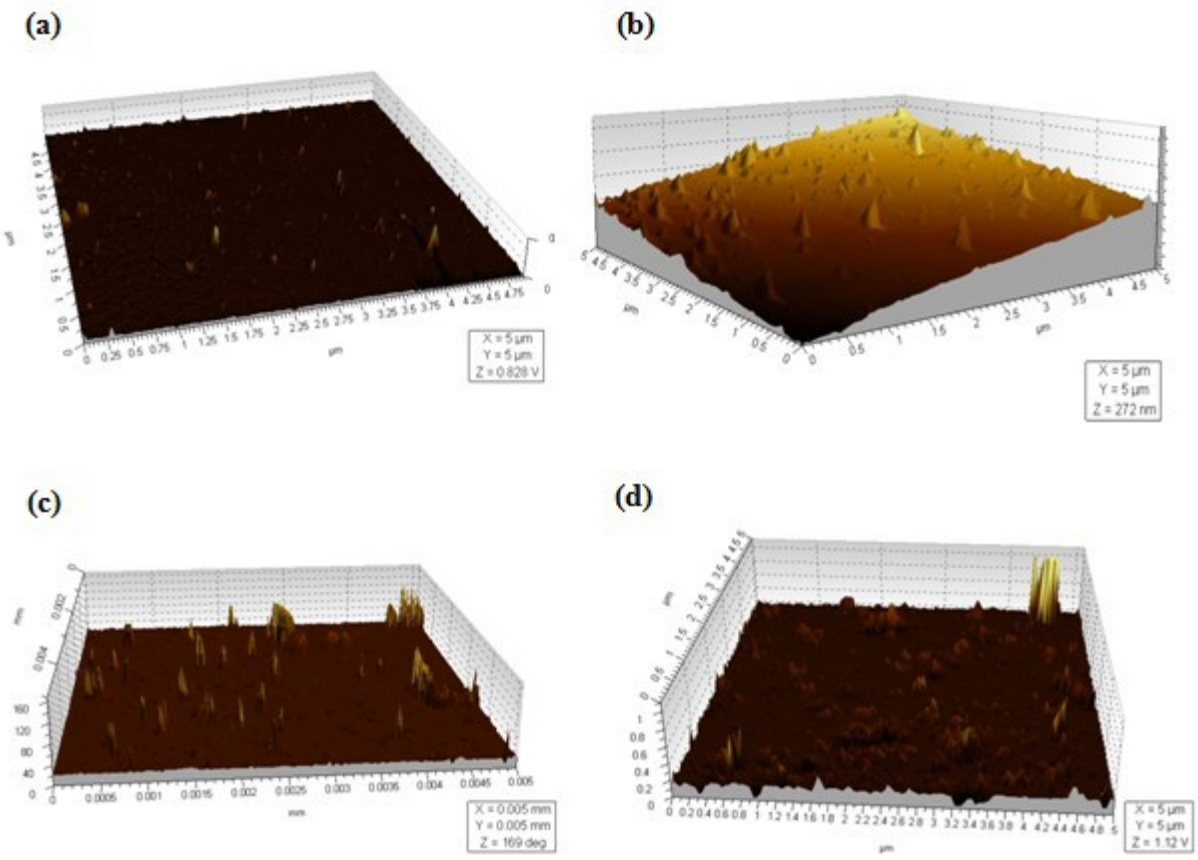

Figure 4.11. 3D picoview images generated from AFM scan images. a) Untreated b) Acetic acid treated c) hydrochloric acid treated and d) sulfuric acid treated. Scan sizes are 5 µm × 5 µm

Table 4.3 shows the results of average diameter and height, after the carbon nanofibers were treated with respective acids. From the table it was clearly evident that all except acetic acid corroded to certain extent. While the Hydrofluoric acid was the most corrosive substance in terms of changes in height of the fiber, it didn't affect the diameter of the fiber more than 10%. Hydrochloric and Sulfuric acids decreased the height of the fiber while the acetic acid increased the height of the fiber. While sulfuric acid increased the diameter of the fiber, acetic and hydrochloric acids decreased the diameter of the fiber.

Table 4.3 Dimensions and Corrosion Rates of Untreated and Acid Treated VACNFs

Acid Used	Average Diameter	Average Height	Corrosion rate (height) nm/min
Untreated	204.7	20.4	-
HCl	180.6	10.9	-1.9
HF	205.5	8.4	-2.4
H_2SO_4	306.9	12.5	-1.6
CH_3COOH	150.6	24.8	+0.9

Average height and diameter are in nm.

It is well known that acids oxidize materials and is even true for carbon nanofibers. Hence the possible mechanism might be that the acids have oxidized the VACNFs and might have led to a decrease in the height of the nanofibers. It should be noted that all three strong acids i.e, HCl, HF and H_2SO_4 caused reduction in height supporting the hypothesis of strong oxidation leads to the particle removal and thus the decline in height. It should be noted that the nanofibers were on a SiO_2 surface and HF etches the SiO_2 surface. Hence the overall change in height was sum of change is height of nanofiber and the change in SiO_2 thickness. Since there was no available data of surface etch, it was concluded that the actual nanofiber etch rate using

HF was more than the value in the Table 4.3. On the other hand, CH_3COOH a weak acid, might have caused weak oxidation of the nanofiber and the excessive acid might have bonded to form a complex which might have increased the height of the fiber. The results were statistically analyzed.

SEM images of the etchant treated substrate surfaces were obtained to further verify the presence of carbon nanofibers. For this purpose, a Philips EL 20 SEM was used at 10^{-5} mBar and shooting an electron ray of 30 KeV. All the images scanned were 10 µm × 10 µm. Figure 4.12(a), (c) and (e) shows the SEM images that were generated from the etchant treated substrates. Energy Dispersive Spectroscopy (EDS) was performed to verify the composition of the etchant treated surfaces. Figure 4.12(b), (d) and (f) shows EDS spectrum images of the etchant treated surfaces. Figure 4.12(a) shows the Hydrochloric Acid treated surface. VACNFs were clearly observed as the illuminating dots in the Silicon Dioxide (SiO_2) which formed the dark background. EDS was then performed on the surface and the EDS spectrum is shown in the Figure 4.12(b). Clearly from the spectrum, peaks for Carbon (C), Oxygen (O) and Silicon (Si) were seen. Since the substrate surface was of SiO_2, both Silicon and Oxygen had the highest peaks and was seen in the spectrum. Figure 4.12(c) shows the SEM image of the sulfuric acid (H_2SO_4) treated surface. VACNFs were seen as the illuminating dots in the image. EDS was then performed on the surface to further verify the composition of the surface and is shown in Figure 4.12(d). The acetic acid (CH_3COOH) treated surface was scanned under the SEM and the image generated is shown in the Figure 4.12(e). EDS of the surface was then performed and is shown in Figure 4.12(f). From the SEM scan images, it was clearly seen that Acetic acid treated surface retained maximum number of fibers and sulfuric acid had an adverse reaction on the surface of the chip and even the fibers became bulged after the treatment with the sulfuric acid. From the

EDS spectrum peaks of Carbon, it was concluded that acetic acid treated surface has the highest Carbon peak and sulfuric acid treated surface has the lowest peak. The results of dimensions also accord this fact as acetic acid treated surface had the height increment and thinning of diameter. Also another reason for the observed peaks was the fact that the acetic acid treated surface had retained the most nanofibers compared to other acid treated surfaces.

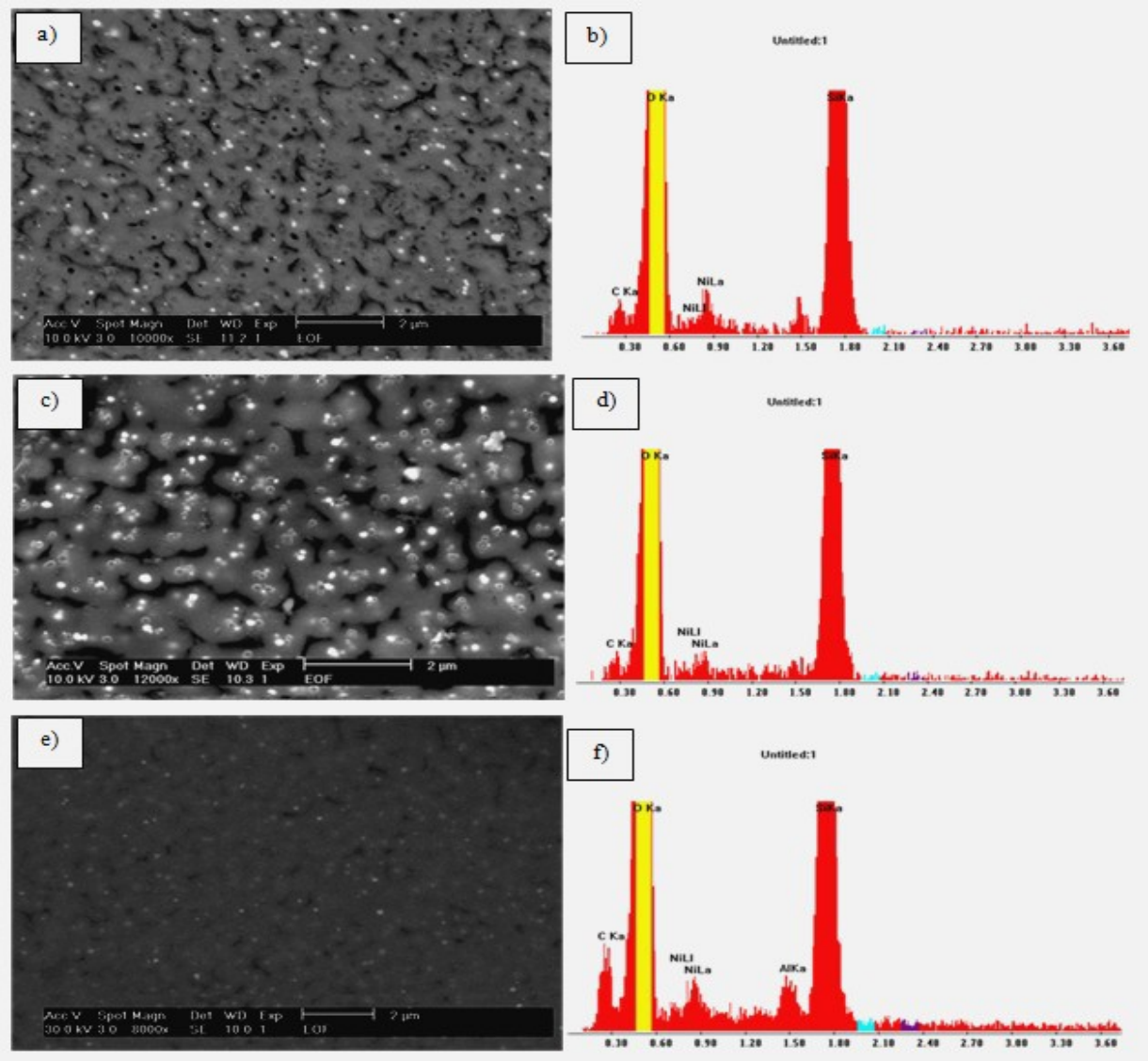

Figure 4.12. a), c), e) SEM scan images of the acid treated surfaces. b), d), f) EDS performed on the scanned surface to get the composition. a) HCl treated substrate surface as seen in the SEM. b) EDS performed on the HCl etched surface. c) H_2SO_4 etched substrate surface as seen in the SEM. d) EDS performed on the H_2SO_4 etched surface. e) Acetic Acid etched substrate surface as seen in the SEM. f) EDS performed on the Acetic Acid etched surface

4.3.5. Statistical Analysis

The collected data was then statistically analyzed for confidence as done in the chapter 3. Confidence interval was calculated at 95% confidence and the overall results for different acids are tabulated in Table 4.4. As seen from the table, the confidence interval is within 20nm for diameter and within 3 nm for the height. This showed the measured values were precise and accurate.

Table 4.4 Calculation Results of CI for the Sizes of Untreated and Acid Treated Nanofibers

		Confidence Interval	Mean	Std Dev.
Unetched	Diameter	[199.9 211.2]	205.5	25.0
	Height	[18.8 22.1]	20.4	7.2
HF Etched	Diameter	[199.2 211.9]	205.5	28.1
	Height	[7.7 9.1]	8.4	3.0
HCl Etched	Diameter	[176.1 185.1]	180.6	20.5
	Height	[9.9 11.8]	10.7	4.3
H_2SO_4 Treated	Diameter	[296.4 317.5]	306.9	46.7
	Height	[11.9 13.1]	12.5	2.4
CH_3COOH Treated	Diameter	[147.5 153.8]	150.6	14.0
	Height	[22.8 24.7]	22.7	4.3

All dimensions are in nm.

Mean and standard deviation values are presented in Table 4.4 from which one can see the accuracy of the measurement.

4.3.6 Conclusion

From the corrosion study it was concluded that the VACNFs were not corrosion resistant. Furthermore, all strong acids resulted in a decrease in height of the fiber while a weak organic acid i.e., acetic acid (CH_3COOH) caused an increase in the height of the carbon nanofibers. The

increase in the height of the CNFs when treated with acetic acid may be due to a partial oxidation initially, leading to the formation of acid functionalized nanofibers which then reacted with the remaining acetic acid to form a bonding and thus increase in the height.

5. NANOCOMPOSITES

5.1 Introduction

Nanocomposites are different combinations of nanomaterials combined to enhance the overall material properties. A nanocomposite by definition is the engineering of two or more naturally occurring elements that have significant physical and chemical properties at nanoscale. Conductive polymers are long known to the scientific community but because of their mechanical instability and other weaknesses, they have not received much attention. But after the works of Ajayan et al [80] and the substantial works showing that composites developed using Multi Walled Carbon Nanotubes (MWCNTs) and polypyrrole (Ppy) showed improved mechanical and physical characteristics [81,82], it has drawn attention from the scientific community. Since then, many tried to build new and novel composites using conductive polymers and were successful in the development of the composites. Inspired by these works, this work investigated novel nanocomposites whose materials and methods are discussed in the following sections.

5.2 Materials and Methods

Acid (-COOH) functionalized Multi Walled Carbon Nanotubes (MWCNTs) with a diameter of 10-20 nm and greater than 95% purity were bought from US Nanolabs. All other chemicals used in the experiment - Thionyl Chloride (>99% purity), Polypyrrole (Ppy > 99.9% purity), Nitric acid, poly alkyl thiophene (Ptp >99% purity) and nanosperse surfactant - were bought from Sigma-Aldrich Inc. Distilled water used in the experiments was from the Millipore DI water system.

All experiments were carried out in a fume hood. A bench top sonicator was used to sonicate the solution for 60 minutes for even distribution. A Micro Toledo Weighing Machine with a precision of 0.01mg was used for measuring the substances. A Beckman Coulter Microfuge was used to centrifuge the samples. An Agilent N5781 DC power supply was used to supply the DC power. An Olympus fluorescent microscope and an Agilent pulse generator were used to carry out the dielectrophoresis.

5.2.1. Preparation of Acyl Chloride functionalized Carbon Nanotubes (COCl-CNT)

Using 10% W/V thionyl chloride and refluxing continuously at 80^{o}C for 3 hours, -COOH functional groups were converted to -COCl functional groups. This step is called the acylation step. After the acylation step, the sample was centrifuged at 12,000 rpm for 30 minutes in order to separate the COCl-CNT from the remaining thionyl chloride. While thionyl chloride was the supernatant, COCl-CNT was precipitated as pellets. The pellets were thus washed with water and then suspended in distilled water, and the stock concentration of 10mg/ml was prepared.

Stocks of COOH-CNT and COCl-CNT were prepared at 10mg/ml and a stock of polypyrrole (Ppy) was prepared at 0.5 M. Poly alkyl thiophene (Ptp) was used at a concentration of 10% W/V. Nanosperse, a surfactant, was added to the COOH-CNT and COCl-CNT stocks, and then the stocks were sonicated using the ultrasound sonicator for 1 hour. The final solutions were then made using the stock concentrations. Both COOH-CNT and COCl-CNT were used at a concentration of 1 mg/ml and conductive polymers were used at stock concentrations. The final solutions were sonicated before carrying the polymerization step.

5.2.2. Polymerization

An electrolytic cell was constructed in a centrifuge tube by drilling holes in the cap with the help of a Dremel tool. Using a diamond tip spinning at a speed of 6000 rpm, fine holes were drilled into the centrifuge tube. With an Aluminum rod as cathode and a Zinc rod as anode, and supplying a power of 1V DC, a 1:1 mixture of COOH-CNT and Polypyrrole (Ppy); 1:1 mixture of COOH-CNT and Poly alkyl thiophene (Ptp); 1:1 mixture of COCl-CNT and polypyrrole (Ppy) and 1:1 mixture of COCl-CNT and poly alkyl thiophene (Ptp) were polymerized for 75 minutes. An Agilent DC power supply was used to supply the 1 V DC power.

From the preliminary observations, while there was no visible color change after the addition of polypyrrole to COOH-CNT or COCl-CNT, there was a color change in the poly alkyl thiophene addition. While the addition of poly alkyl thiophene to COOH-CNT resulted in a white color, addition of poly alkyl thiophene to COCl-CNT resulted in light blue color.

After the polymerization, the samples were centrifuged and resuspended in Fresh DI water in order to remove the excess conductive polymers.

5.3 FTIR Spectroscopy Studies of Nanocomposites

After the composites were prepared, they were coated onto a double sided polished Si surface as a thin film. In order to deposit a thin film, 200 µl of sample was spread on the Polished Si surface and dried on the hotplate at 80^{o}C for 15 seconds in order to evaporate the liquid. Once the liquid was evaporated completely, the sample was dried in the dry box until the relative humidity fell below 5%. The samples were then measured using Fourier Transform Infrared Spectroscopy (FTIR) spectroscopy.

FTIR spectroscopy relies on the principles of light absorption of molecules in the infrared regime. Each molecule has its own absorption/transmittance range depending on the types of bonding and the internal lattice structural arrangement. It has been used in the past as an effective tool for the verification of new composites, as the absorption is specific for each molecule. Thus it was used in the current experiment to validate the bonding between the conductive polymer and the COOH/COCl functionalized Multi Wall Carbon Nanotubes (COOH-MWCNTs). FTIR scans were obtained using double side polished Polysilicon as the reference. The results of the FTIR scan are shown in Figures 5.1 and 5.2.

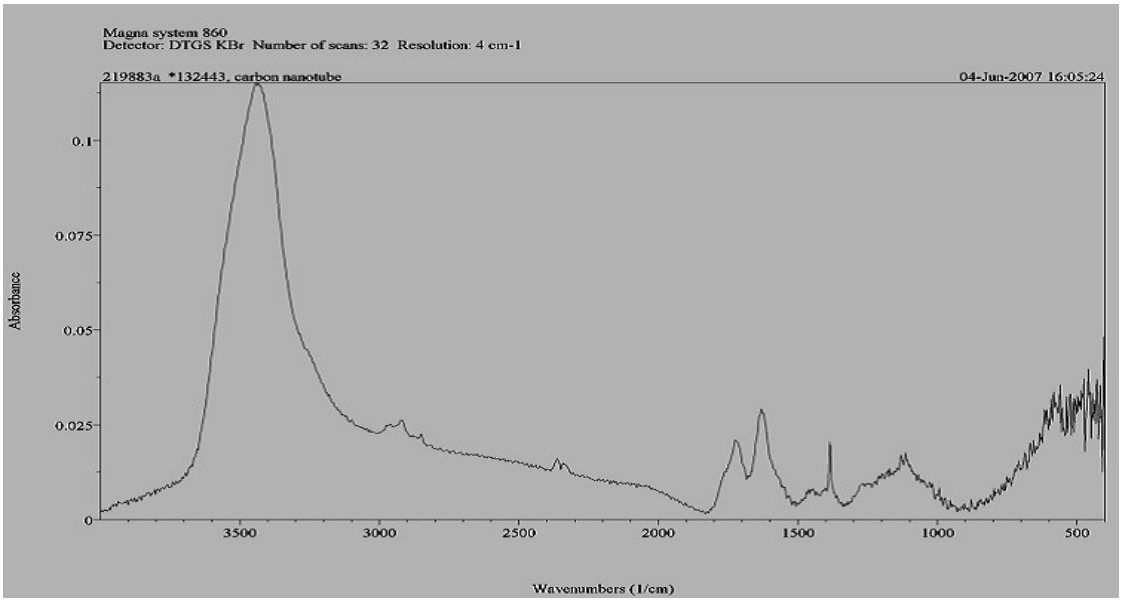

Figure 5.1. Absorbance peak of the COOH-CNT using FTIR spectroscopy, Image retrieved from the vendor's data sheets.

Figure 5.1 is an adaption from the vendor who sold the COOH- CNT samples. The sample was scanned with KBr taken as a reference. From the graph it was clearly observed that the COOH-CNT peaked at a wavelength of 3500 cm^{-1}. Since the composite was in the liquid medium, it was coated as a thin film on the polished Si surface, and readings were then recorded.

Figure 5.2 shows the FTIR results after the polymerization. The two peaks that were observed for the bonding were shown in orange dotted lines.

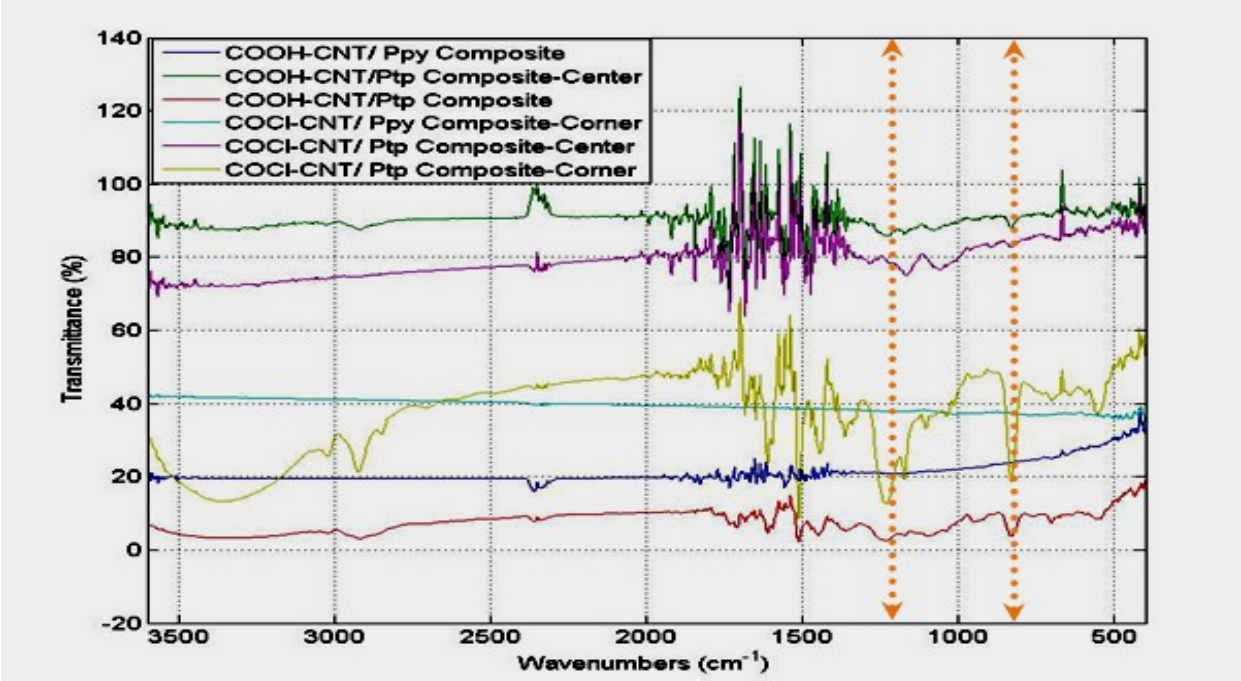

Figure 5.2. Matlab generated image of the FTIR collected data for the polymerized nanocomposites.

Based on the experimental results in Figure 5.2, it was clearly evident that, except in the COCl-CNT and Ptp composite, no other curve had a peak closer to 3500 cm^{-1} wavelength, suggesting that there was no free CNT-COOH in the medium. Large noise was observed at around 1600 cm^{-1} which was due to the absorption of polished Si substrate and the air medium. New peaks were observed in the 900 cm^{-1} region corresponding to polymer ring deformation, and in the 1200 cm^{-1} region corresponding to C-H in plane bends. One must also note that the absorption bands were sensitive to levels of oxidation. Therefore, it was confirmed from the FTIR spectroscopy images that the bonding had taken place in the nanocomposite samples.

5.4 Dielectrophoresis of Nanocomposites

The newly developed nanocomposites were then deposited onto the microelectrode using the dielectrophoresis technique. Dielectrophoresis is a technique of driving dielectric materials and aligning them in an uneven electric field. The applied force is directly dependent on the electrode potential. The overall experimental setup is shown in Figure 5.3. As shown in the Figure 5.3, the microelectrode contact pads were bonded to wires using conductive epoxy and these wires were connected to the oscilloscope from which a sinusoidal wave with 1.5 MHz frequency and 30 V_{P-P} voltage was applied. Once the voltage was applied to the system, 1.5 µl of the sample was pipetted out using the micropipette and carefully positioned at the microelectrode. Once the addition of the droplet was complete, the function generator was turned on and left for about 30 seconds to complete the dielectrophoresis.

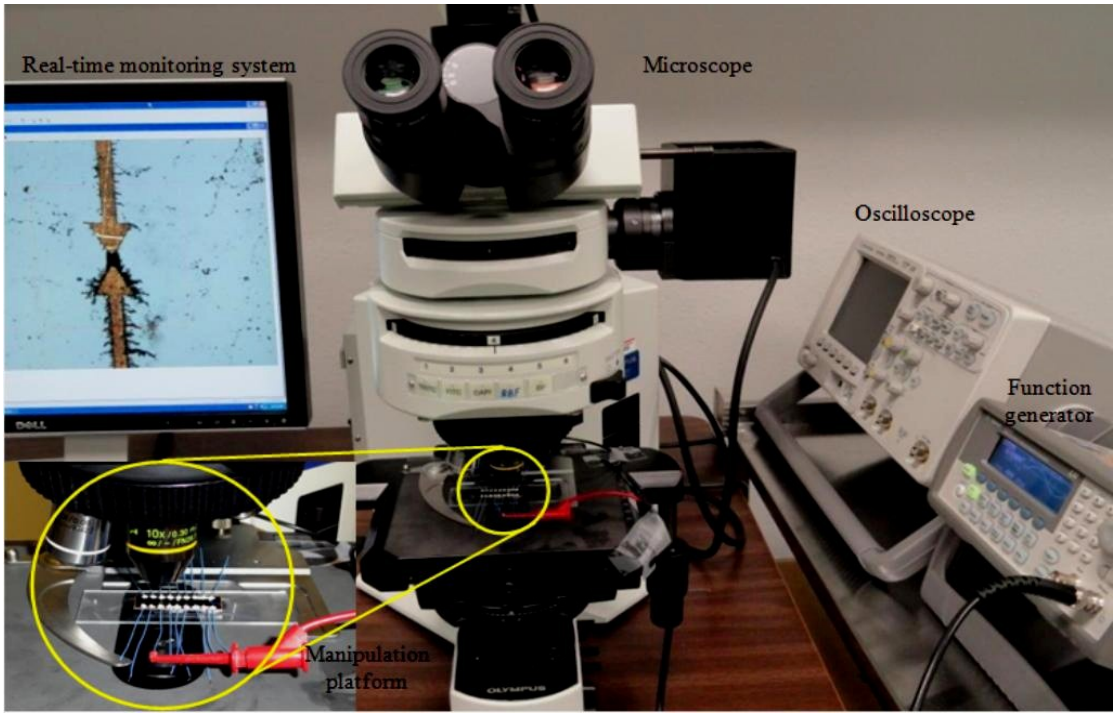

Figure 5.3. Experimental setup for dielectrophoresis.

Bulk CNT movement was observed using the optical microscope. Thus after sufficient movement of the particles was achieved as seen from the optical microscope, power was turned off and the remaining liquid was allowed to dry. The experiment was then repeated for all other nanocomposites. After the dielectrophoresis, the electrical properties of the newly developed nanocomposites were analyzed by plotting an I-V characteristic curve and calculating the overall resistance of the newly developed nanocomposites.

The surface was then scanned for the CNT composites using the Philips XL 20 Scanning Electron Microscope (SEM). The scan images of the electrodes after the dielectrophoresis are shown in Figure 5.4.

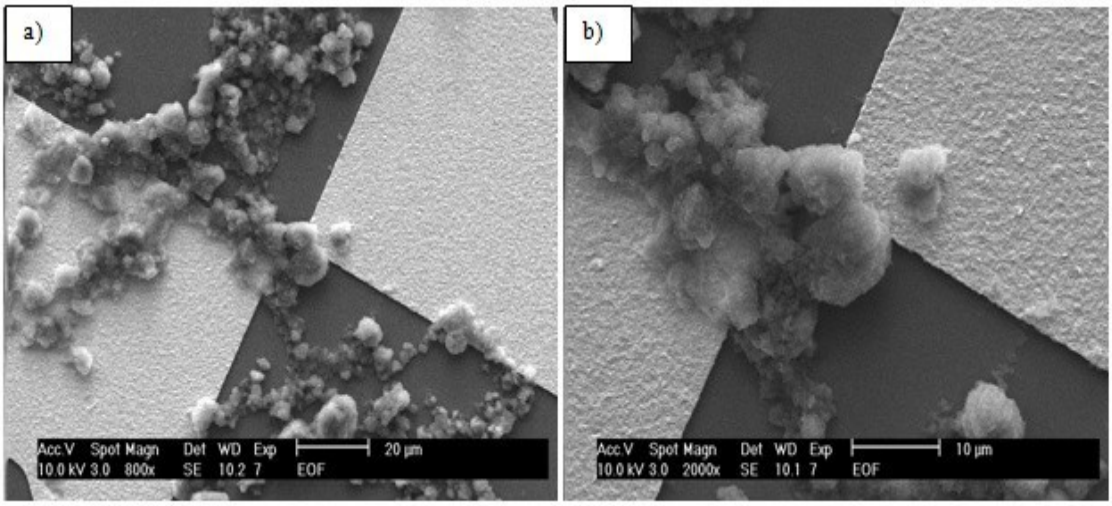

Figure 5.4. SEM Images of the electrodes after the Dielectrophoresis. Nanocomposite bundles are clearly visible as bridging the electrodes. a) 20 µm scan area b) 10 µm scan area

As seen in the Figure 5.4, bundles of the nanocomposites bridged the electrodes after performing the dielectrophoresis. SEM images showed bundles of nanocomposites unlike the acid functionalized (-COOH) CNTs. It was observed that there was faster movement of the

nanocomposites to the center than the acid functionalized CNTs. Electrical resistance was measured by doing an I-V curve on the electrode.

For obtaining the I-V curve data, a multimeter and a DC power source was used. Using DC power source, a constant DC voltage in the range of 0-5 V with an increment of 1 V was supplied through the electrodes and the current was measured using an ammeter. The results of the I-V curve measurement for all the nanocomposites are tabulated in Table 5.1 and a graph of I versus V is plotted in Figure 5.5.

Table 5.1 I-V Curve Measurements Made For the Nanocomposites after the Dielectrophoresis

Voltage (V)	Current (A)				
	CNT-COOH	COOH-CNT/Ppy	COOH-CNT/Ptp	COCl-CNT/Ppy	COCl-CNT/Ptp
0	0	0	0	0	0
1	0.00000241	0.00006970	0.00000318	0.00000614	0.00000353
2	0.00000431	0.00014450	0.00001609	0.00001355	0.00000728
3	0.00000656	0.00021738	0.00003577	0.00003980	0.00001000
4	0.00000886	0.00031893	0.00006410	0.00005812	0.00001320
5	0.00001117	0.00042318	0.00009059	0.00008324	0.00001428

From the I-V curve, the slopes which were the conductivities of the polymer composites were calculated and compared with the COOH functionalized CNTs. Because of the bundles attachment at the microelectrodes as seen in Figure 5.4, it was not practical to estimate the actual length and area of the nanocomposites in between the electrodes. As the device geometry causes variation in the conductivities, no conclusion was drawn about the conductivities in this work.

Table 5.2 gives the conductances of the nanocomposites made by different functionalized CNTs and their corresponding conductances.

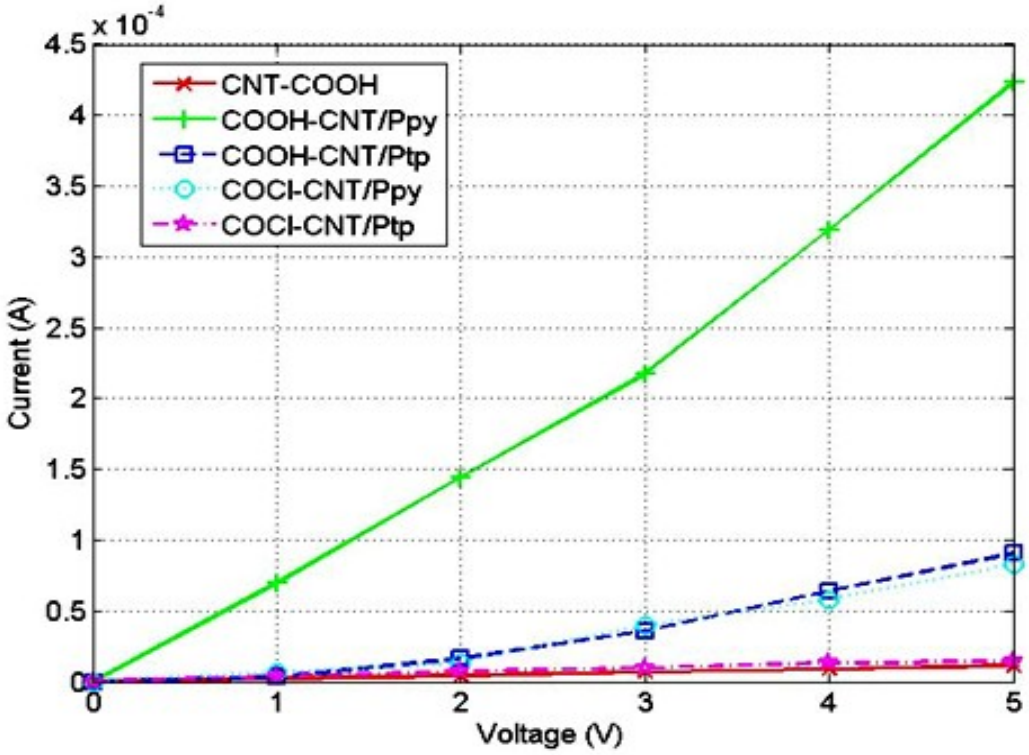

Figure 5.5. I-V Curve Graph for the nanocomposites

Table 5.2 Conductivities Calculated From the I-V Curve

Material	Conductance (mho)
CNT-COOH	2.2129×10^{-6}
CNT-COOH/Ppy	8.3899×10^{-5}
COOH-CNT/Ptp	1.8725×10^{-5}
COCl-CNT/Ppy	1.7097×10^{-5}
COCl-CNT/Ptp	2.9466×10^{-6}

The Ppy-CNT composite, prepared by the COOH functionalized as well as COCl functionalized polymerization resulted in a forty fold decrease in the resistance of the material.

While Ptp nanocomposite synthesized using -COOH functionalized CNT has an increased conductivity, the same composite synthesized using the COCl functionalized group does not have change in the overall resistance.

5.5 Electrode deposition of Carbon Nanotubes and other Nanocomposites

The nanocomposites were coated onto a copper electrode using an electro-deposition technique. In this technique, the electrode was placed in the nanocomposite containing solution and a pulse voltage of 1.5 V_{p-p} at a frequency of 1 KHz was passed through the cell, and the electrodes deposited were dried in the air for 24 hours before scanning to observe the deposition. The dried electrodes were then scanned using a Philips XL 20 SEM. The samples were scanned at 10 KeV and at a pressure of 1×10^{-5} mbar. The scanned SEM images are shown in Figure 5.6.

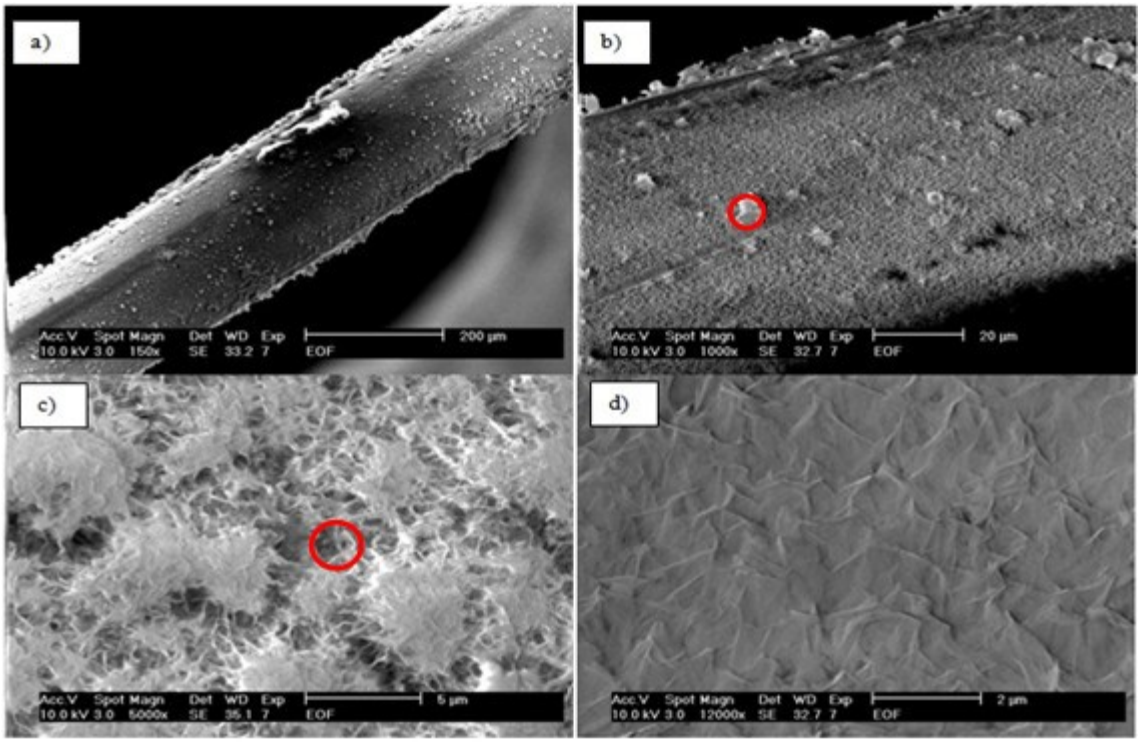

Figure 5.4. Copper electrode deposited with COOH-CNT-Ptp nanocomposite. a) 200 µm scan area clearly showing a thin layer of deposited nanocomposite. b) 20 µm scan area which clearly shows the deposited nanocomposite as a thin layer c) 5µm scan area showing the nanocomposite bundles and d) 2µm scan area showing the composite.

From the Figures 5.6 (a), (b), (c) and (d), coatings were clearly seen on the copper electrode. Bundles of the nanocomposites were seen at a resolution of 5 µm and at 2 µm. But since the carbon nanotubes were of 20 nm in diameter, no conclusion on the carbon nanotubes presence was drawn from these images.

5.6 Conclusion

Nanocomposites were successfully developed and deposited onto the electrode. Dielectrophoresis was successfully employed for bridging the nanocomposites in between microelectrodes and the resistances of the newly developed composites were measured. Assuming the dimensions of all bridged nanocomposites and the acid functionalized MWCNTs was same, nanocomposites had conducted better than MWCNTs.

6. PICOLITHOGRAPHY

6.1 Introduction

With the advent of MEMS and microsensors, device dimensions started to shrink. This shrink in dimensions created a challenge to researchers to create equipment that can work effectively micro and nanoscale materials. Picolithography is one such tool developed in AFMs to create nanochannels. This was previously used to mechanically micromachine nanochannels on substrates such as polymers, metals, semiconductors and insulators [83, 84] but was never used before to create channels on poly silicon surface. Polysilicon surface scratching was performed using the AFM based Picolithography. This method uses a hard tip to scribe the surface repeatedly and the scribing will create a channel. One advantage with AFM based Picolithography is that it needs only single equipment for creation and measurement and doesn't need any pre or post processing as in the case of other fabrication techniques. But the Picolithography also poses a problem of residual accumulation and being unreliable in repetition. Thus in this work nanochannel creation using the atomic force microscope was explored and carbon nanotubes were deposited in the channel using dielectrophoresis. This structure could lead to development of novel devices with the Carbon nanotube integration as bridges.

6.2 Experimental Setup

6.2.1 AFM Based PicoLITH:

The AFM was used to create the nanochannels with the overall schematic of the working procedure shown in Figure 6.1. As shown in the schematic, the applied setpoint voltage controlled the overall force applied by the cantilever on the substrate surface. The software driven cantilever was used at that particular setpoint voltage to repeatedly scratch on the surface

which created a nanochannel. In order to avoid damage to the substrate surface during measurements, scanning the surface was done in tapping mode while the scratching was done in contact mode with closed loop enabled. The Tap190DLC probe tip with a resonant frequency of 190 KHz and a force constant of 48 N/m was used for the scratching.

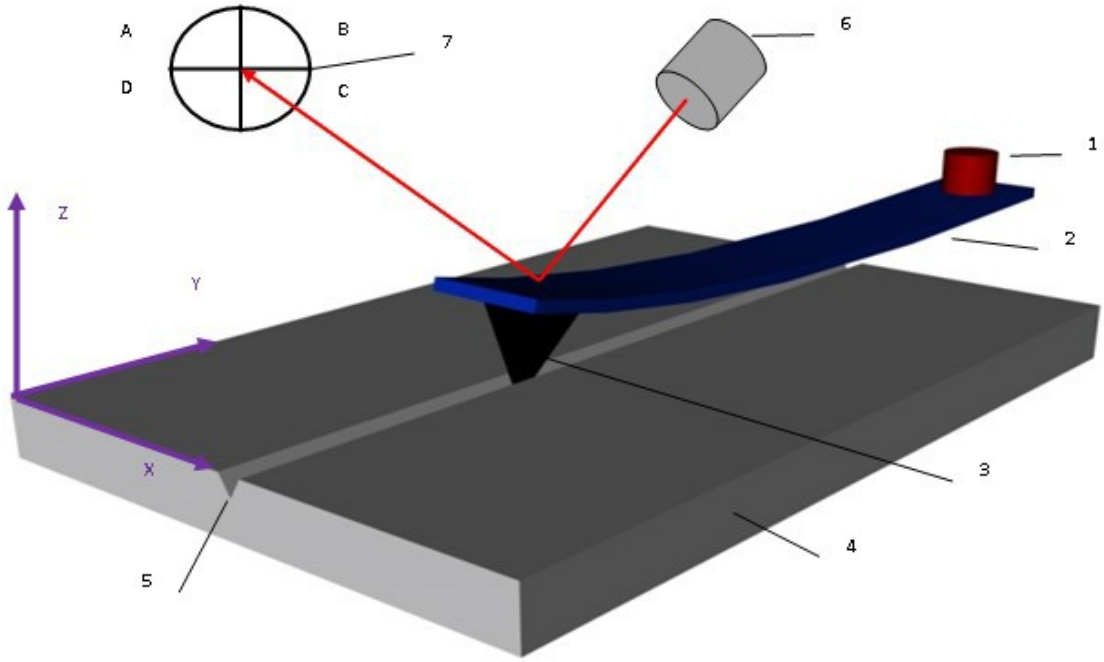

Figure 6.1. Schematics of nanoscratching: (1) piezo scanner for XYZ movement; (2) cantilever; (3) diamond tip; (4) silicon; (5) nanochannel; (6) laser; and (7) four-quadrant PSD

A scan of the topography was done before proceeding with the Picolithography. Then the image was loaded into the software called the picoLITH and markings were made and a 2 V set point voltage and 1 µm/sec cut speeds were fed into the system. Then the operation was performed in a closed loop in order to have an accurate cut as the scanner used feedback control to position the tip. The surface was then rescanned in the tapping mode to make sure that there was a cut on the surface. The probe used in this experiment having a force constant of 48N/m could cause irreversible damage to the chip. For this force constant, a setpoint voltage of 2 V was

applied. Scratching on the Mica surface for calibration resulted in a sensitivity of 66.5 nm/V. Thus the applied tip force was 7 µN (Tip force = 2 × 66.5 × 48). Hence, much careful attention should be taken in order to complete the scanning and scratching.

6.2.2 Results and Discussion

Figure 6.2 shows the scratching done on silicon dioxide (SiO_2) surface using the DLC probe tip at a constant cut speed. Figure 6.3 shows the 3D image generated using the picoimage of the AFM software. A nanochannel was seen in the 3 D image generated by the picoimage.

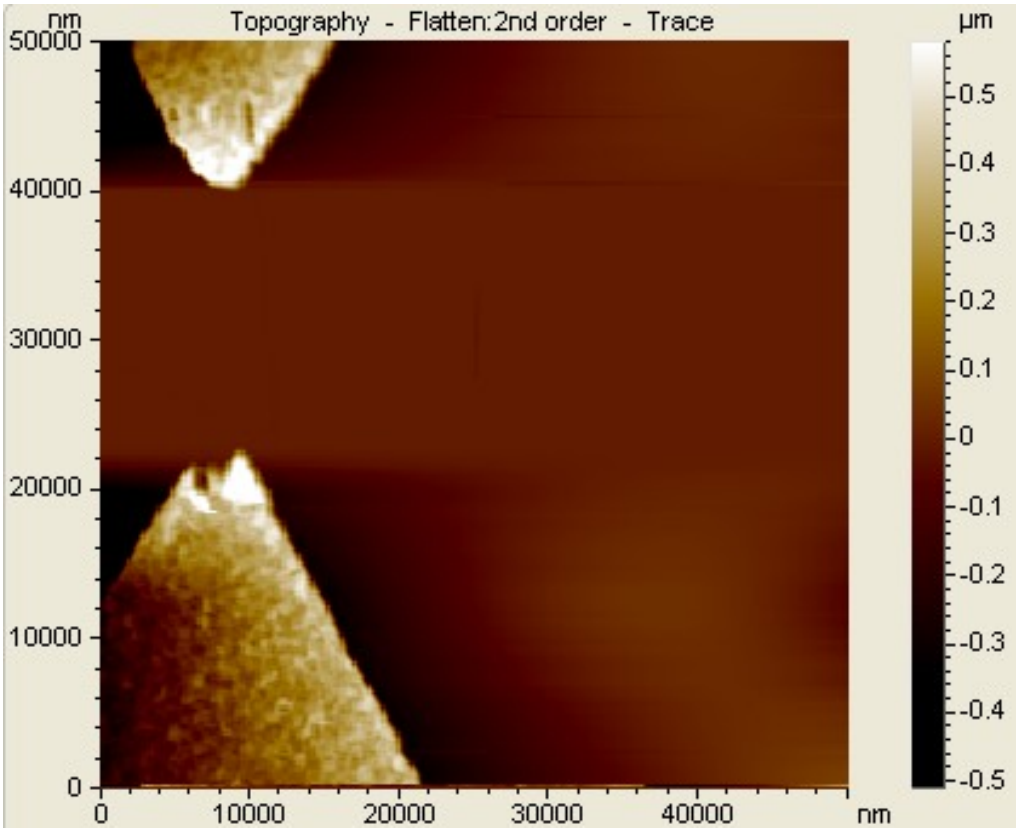

Figure 6.2. AFM topography scan of a pair of electrodes before scratching

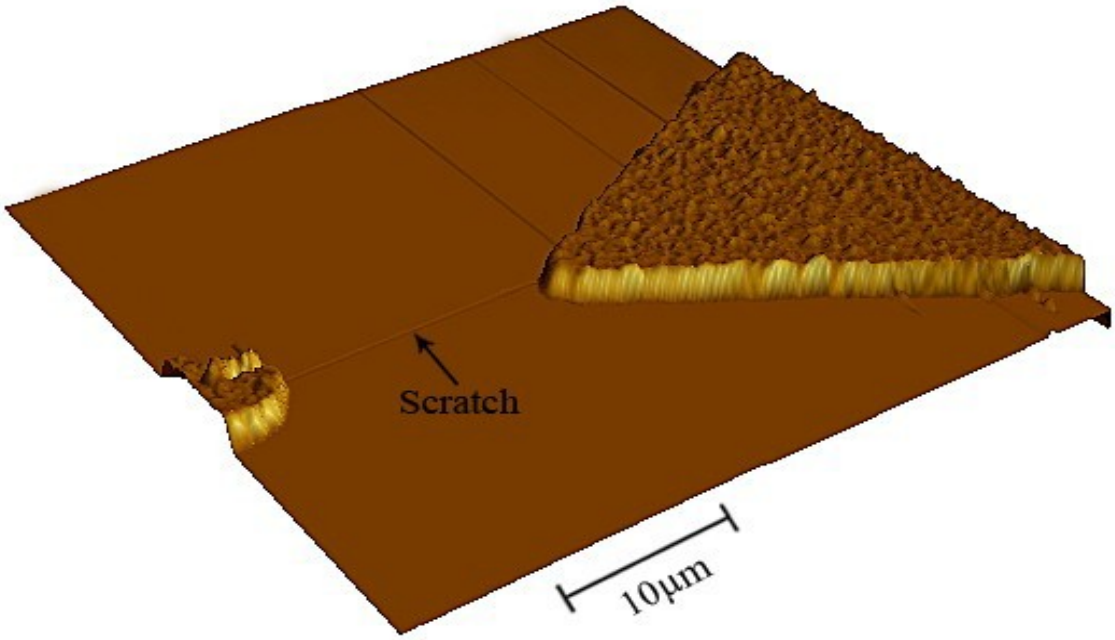

Figure 6.3. 3D topography image of a pair of electrodes with scratched gap.

After the rescan, the channel width and depth were measured by drawing a cross section line across the channel. A cross sectional scan of the channel was shown in Figure 6.4. The channel depth was obtained from the vertical axis and the channel width was obtained from the horizontal axis. Figure 6.4 was obtained by drawing a 1.75 µm length line over the scanned surface.

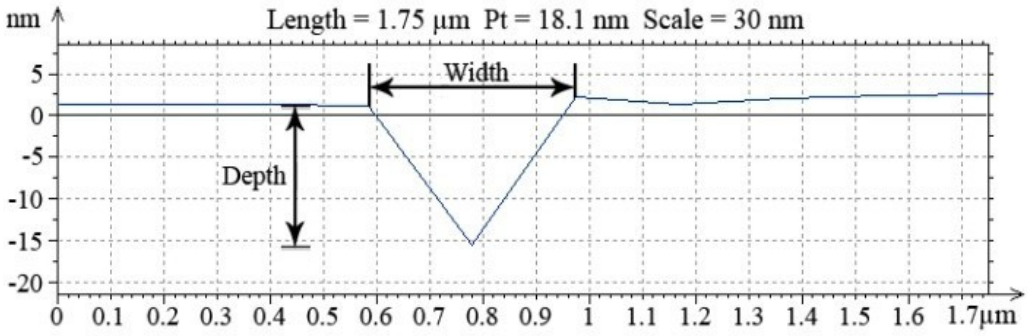

Figure 6.4. Dimension measurement of the scratched nanochannel

Table 6.1 Dimension Measurement Results of Scratched Nanochannels

Elec. Pair #	Tip force (µN)	# of passes	Length (µm)	Width (µm)	Depth (nm)
1	7	150	17.32	0.58	2.8
2	7	150	21.88	0.39	2.1
3	7	150	18.16	0.59	4.9
4	7	150	18.75	0.59	9.1
6	7	150	21.09	0.78	3.4
7	7	150	17.97	0.39	4.2
8	7	150	18.95	0.39	16.8
9	7	150	19.14	0.39	1.8
Average	7	150	19.16	0.51	5.6

Channels were scratched onto the microelectrodes using the AFM based picoLITH and the average for 9 different scratches with same cut speed of 1 µm/sec was given in Table 6.1. Note that each electrode was cut for 150 times. After the scratching, the channels were bridged with the CNTs using dielectrophoresis technique.

6.3 Dielectrophoresis

Dielectrophoresis was carried out with Single and Multiwalled Carbon Nanotubes (CNTs) according to the procedure done in the Chapter 5. Figure 6.5 shows different stages in the DEP process during the deposition of CNTs. Figure 6.5(a) shows the microelectrode before the DEP was carried out and the gap length was measured and found out to be 13.65 µm. Then a 10X dilution of 1 mg/ml CNT solution was made, 1.5µl of the solution was carefully pipetted out and added as a drop onto the surface of the electrode. The solution added electrode surface was shown in Figure 6.5(b). After the solution was added, a sinusoidal AC power was supplied at 20 V_{p-p} and the system was left for about 30 seconds in order to complete the process. Bridged single and multi walled CNT electrodes were shown in the Figures 6.5(c) and (d) respectively.

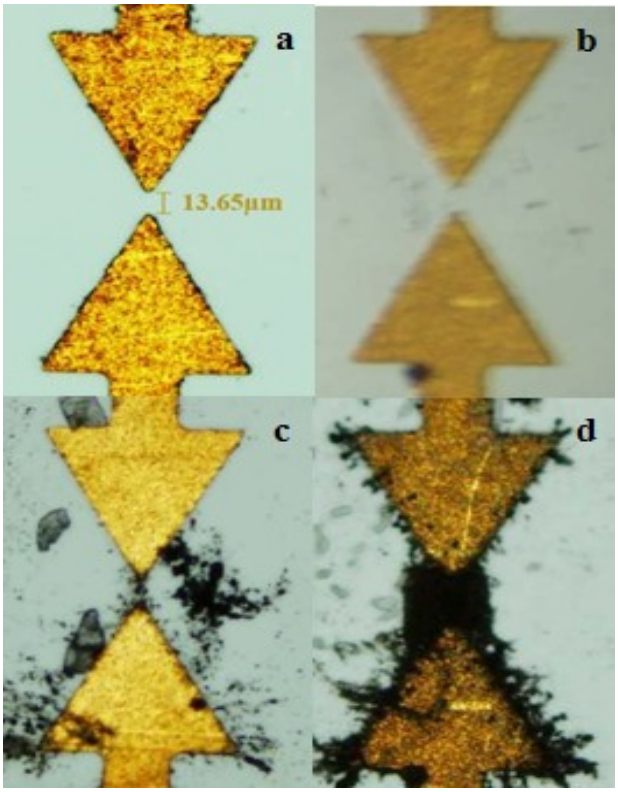

Figure 6.5. Pairs of Au electrodes observed by optical microscope: a. gap measure; b. covered by tiny CNT droplet; c & d. bridged by SWCNTs and MWCNTs respectively.

After the bridging of the electrodes using the DEP process, an I-V curve was constructed using the DC power supply and multimeter in order to verify the resistance data for the carbon nanotubes to verify the bridging and find the resistance of the carbon nanotubes (CNTs). The results of the I-V curve were shown in the following sections.

6.4 Results and Discussion

After the dielectrophoresis, bridging between the electrodes was verified through the resistance measurement. As SiO_2 was the material on which the gold electrodes were deposited and as SiO_2 was an insulating layer, the resistance will be close to infinite unless the CNTs form a bridge. For accuracy, an I-V plot was constructed for each electrode. The results of the I-V

curves plotted for each pair of electrodes were shown in Figure 6.6. Pairs 1-3 were bridged with Single walled CNT and pairs 5-8 were bridged with Multi walled CNT. Pair 4 was bare electrode without any CNT deposition and was taken as reference.

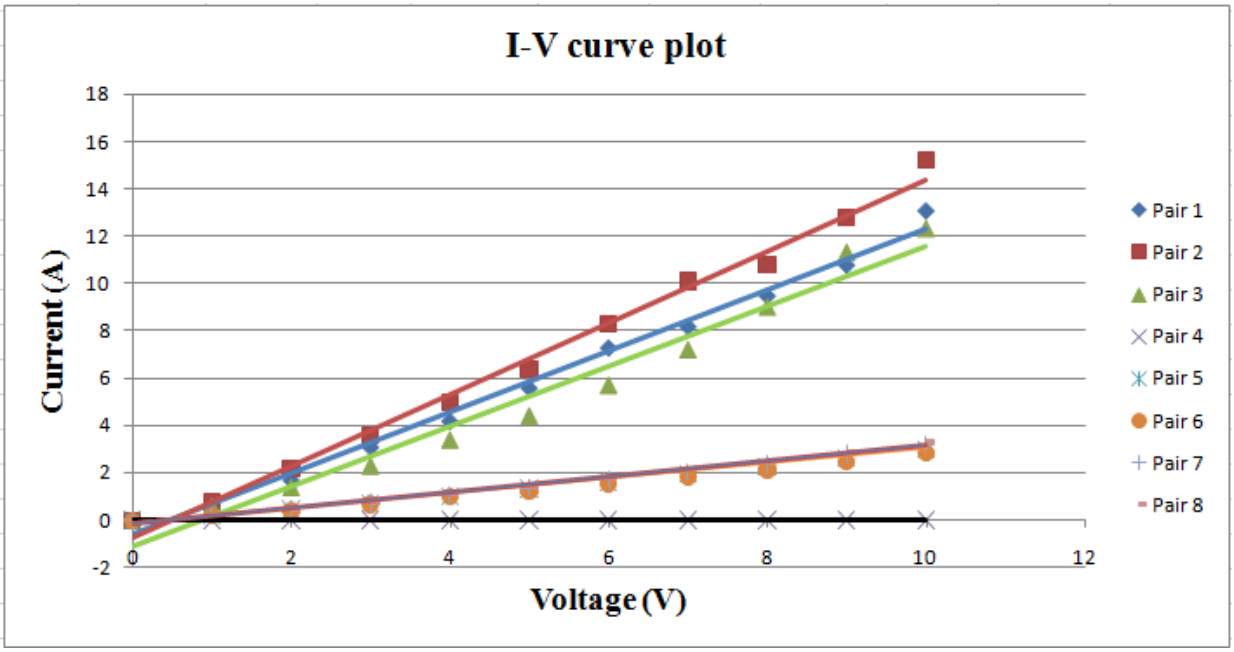

Figure 6.6. I-V curve measurement with SWCNTs alignment (Pair 1-4) and MWCNTs alignment (Pair 6-9) in the scratched gaps. Pair 5 is for the bare electrode.

From the I-V curve results, it was observed that both single and multi walled CNTs bridge had a linear relationship and since the CNTs were either metallic or semiconducting, it led to a conclusion that both were metallic in nature. The graph also shows that the result was reproduced for all the pairs.

It was theoretically considered that single walled is semiconducting and multi walled is metallic in nature. But contrary to the theory, our results show that both the single and multi walled were metallic. One reason for getting this result might be because of the bundling of the CNTs. This can be avoided by narrowing the channel and performing the dielectrophoresis. Also

cleaning off the surface after the dielectrophoresis to remove off the excess layer of CNTs over the surface might help.

6.5 Conclusion

Microelectrodes were scratched between gold electrodes to create a nanochannel and the dielectrophoresis was used to create a CNT bridge across the electrode gap. The bridged CNTs I-V curve was plotted and the result showed both single walled and multi walled CNTs were metallic. This technique in future can be used to create a channels and CNT bridges.

7. CONCLUSIONS

In all, the behavior of the Vertically Aligned Carbon Nanofibers (VACNFs) from -70^{o}C – 100^{o}C was successfully quantified and statistically analyzed. From the results it was concluded that there was no dimensional change in the ambient temperature zone as the range of data was much scattered and the variance of the data included all of the data points across the temperature range. But there was a dimensional change when the nanofibers were cooled to -20^{o}C and the dimensional data was scattered and the variance included all of the data points in between -20^{o}C and -70^{o}C. This was because of the initial contraction of the nanofibers reaching a minimal lattice configuration. Once this lattice configuration was reached, the internal forces like the lattice energy, electrostatic repulsion would become predominant and resist any further contraction. Furthermore, the results were statistically analyzed for accuracy.

Mechanical properties of the VACNFs were studied from -70^{o}C to 23^{o}C and corrosion of the VACNFs with respect to strong acids was studied. From the experimental results it was concluded that the Young's modulus of the nanofibers have an exponential relation to temperature in the subzero range. Furthermore dimensional changes in the VACNFs at subzero temperatures was quantified. It had been shown that there was a change in dimensions of the nanofibers when compared to the room temperature but the dimensional data included all the data in subzero temperature with variance considered.

CNT – conductive polymer nanocomposites were developed using COOH- and COCl-functionalized CNTs. Developed polymers electrical properties were analyzed by bridging them across microelectrode using Dielectrophoresis technique. A forty fold increase in conductivity

was achieved for the polypyrrole coated carbon nanotubes while a ten fold increase in conductivity was obtained for poly alkyl thiophene coated carbon nanotubes. This data was under the assumption that all the nanocomposites had same geometry that of the microelectrode. Since there was no actual geometric data available, the results were uncertain. It was shown that COCl-functionalized CNTs was not good for polymerization when compared to COOH-functionalized CNTs.

Creation of Nanochannels on the Silicon Dioxide (SiO_2) surface using AFM based picolithography was explored. CNT was bridged along the nanochannel containing microelectrodes. I-V curve was plotted for the bridged Single and Multiwalled CNTs.

8. FUTURE WORK

The present research results will provide research opportunities in the following directions:

1. The current temperature study can be extended to humidity study as well in order to have an even better understanding of the behavior of the carbon nanofibers.
2. Extreme environmental characterization was done for the mechanical properties. Along with mechanical properties, electrical properties do change in the extreme environments. Thus electrical properties of the nanomaterials in the extreme environments need to be studied. Development of novel nanocomposites with ceramic materials can possibly be one of the interesting areas to explore.
3. Corrosivity test was only done on the acids. But there are even alkalis that might cause corrosion. Thus the behavior of the carbon nanofibers to these materials needs to be characterized.
4. Development of Nanocomposites using ceramic materials will help improve the corrosive resistance and extreme environmental tolerance. Thus research needs to pay attention on developing nanocomposite using these with no compromise in the mechanical and electrical properties of carbon nanofibers.
5. Nanocomposites have shown significant improvement in the electrical properties but addition of metals to these might even better the properties and will be an interesting future direction to explore.
6. The deposited electrodes can be used as sensory elements as they will have higher sensitivity. Thus their application in different fields can be explored.

7. Development of CNT bridged ISFET is an interesting thing to explore in near future. CNT tunneling can be explored as well i.e. deposition of insulator on the top of the CNT bridged channel in order to create a CNT tunnel can be explored.
8. Nanochannels created using the Atomic force microscopy on different surfaces can be used in creating micromachines.

BIBLOGRAPHY

[1] T. Bozhi; Z. Xiaolin; K. Thomas J. F. Ying; Y. Nanfang; Y. Guihua; H. Jinlin & Lieber, Charles M. (2007). "Coaxial silicon nanowires as solar cells and nanoelectronic power sources". *Nature* 449 (7164): 885–889. Bibcode 2007Natur.449..885T. doi:10.1038/nature06181. PMID 17943126

[2] X. Jie; L. Wei; H. Yongjie; W. Yue; Y. Hao & Lieber, Charles M. (2006). "Ge/Si nanowire heterostructures as highperformance field-effect transistors". *Nature* 441 (7092): 489–493. Bibcode 2006Natur.441..489X. doi:10.1038/nature04796. PMID 16724062.

[3] J. Fritz, M. K. Baller, H. P. Lang, H. Rothuizen, P. Vettiger, E. Meyer, H.J. Güntherodt, Ch. Gerber, and J. K. Gimzewski; "Translating Biomolecular Recognition into Nanomechanics" *Science 14 April 2000: 288 (5464), 316-318. [DOI:10.1126/science.288.5464.316]*

[4] J. Sniegowski and E. Garcia, "Surface-micromachined geartrains driven by an on-chip electrostatic microengine," IEEE Electron Device Letters, vol. 17, no. 7, p. 366 (1996).

[5] J. Sniegowski, S. Miller, G. LaVigne, M. Rodgers, and P. McWhorter, "Monolithic geared-mechanisms driven by a polysilicon surface-micromachined on-chip electrostatic microengine," Proc. Solid-State Sensor and Actuator Workshop, pp. 178-182 (1996).

[6] X. Gao, L. Yang, J. A. Petros, F. F. Marshal, J. W. Simons and S. Nie; "*In vivo* molecular and cellular imaging with quantum dots" Analytical biotechnology; Volume 16, Issue 1, February 2005, Pages 63-72

[7] F. Allhoff, P. Lin, D. Moore, "*What is nanotechnology and why does it matter?: from science to ethics"*, pp.3-5, John Wiley and Sons, 2010 ISBN 1405175451.

[8] E. Gazit, "Plenty of room for biology at the bottom: An introduction to bionanotechnology". Imperial College Press, 2007, ISBN 9781860946776

[9] G. M. Whitesides, et al. (1991). "Molecular Self-Assembly and Nanochemistry: A Chemical Strategy for the Synthesis of Nanostructures". *Science* 254: 1312. doi:10.1126/science.1962191. PMID 1962191

[10] F. Patolsky; B. P. Timko; G. Yu; Fang, A. B. Greytak; G. Zheng & C. M. Lieber (2006). "Detection, stimulation, and inhibition of neuronal signals with high-density nanowire transistor arrays". *Science* 313 (5790): 1100–1104. doi:10.1126/science.1128640.

[11] S. Das, A. J. Gates, H. A. Abdu, G. S. Rose, C. A. Picconatto, J. C. Ellenbogen (2007). "Designs for Ultra-Tiny, Special-Purpose Nanoelectronic Circuits". *IEEE Transactions on Circuits and Systems I* 54 (11): 2528–2540. doi:10.1109/TCSI.2007.907864

[12] J. Tatebayashi, M. Nishioka, T. Someya, and Y. Arakawa; "Area-controlled growth of InAs quantum dots and improvement of density and size distribution" Appl. Phys. Lett. 77, 3382 (2000); doi:10.1063/1.1327613 (*3 pages*)

[13] J. Hu, Y. Zhang, H. Gao, M. Li and U. Hartman; " Artificial DNA Patterns by Mechanical Nanomanipulation" *Nano Letters* 2002 *2* (1), 55-57

[14] C. Baur, B. C. Gazen, B. Koel, T. R. Ramachandran, A. A. G. Requicha, and L. Zini; "*Robotic nanomanipulation with a scanning probe microscope in a networked computing environment*" J. Vac. Sci. Technol. B 15, 1577 (1997); doi:10.1116/1.589404 (*4 pages*)

[15] W. Kroto, J. R. Heath, S. C. Obrien, R. F. Curl, and R. E. Smalley, Nature (London) 318, 162 (1985).

[16] S. Iijima, Nature (London) 354, 56 (1991).

[17] Z. Li, Y. Xiong, and Y. Xie "Selected-Control Synthesis of ZnO Nanowires and Nanorods via a PEG-Assisted Route" *Inorganic Chemistry* 2003 *42* (24), 8105-8109

[18] C. K. Chan, R. N. Patel, M. J. O'Connell, B. A. Korgel, Y. Cui; "Solution-Grown Silicon Nanowires for Lithium-Ion Battery Anodes" *ACS Nano* 2010 *4* (3), 1443-1450

[19] J. Cai, P. Ruffieux, R. Jaafar, M. Bieri, T. Braun, S. Blankenburg, M. Muoth, A. P. Seitsonen, M. Saleh, X. Feng, K. Mullen and R. Fasel; "*Atomically precise bottom-up fabrication of graphene Nanoribbons*" Nature; Vol 466|22 July 2010| doi:10.1038/nature09211

[20] P. U. Arumugam, H. Chen, S. Siddiqui, J. A. P. Weinrich, A. Jejelowo, J. Li and M. Meyyappan, "Wafer- Scale Fabrication of Patterned Carbon Nanofiber Nanoelectrode Arrays: A Route for Development of Multiplexed, Ultrasensitive Disposable Biosensors", Biosensors and Bioelectronics, 24(2009), 2818-2824.

[21] Y. Y. Fan, A. Kaufmann, A. Mukasyan and A. Varma; "*Single- and multi-wall carbon nanotubes produced using the floating catalyst method: Synthesis, purification and hydrogen up-take*" Carbon, Volume 44, Issue 11, September 2006, Pages 2160-2170; doi:10.1016/j.carbon.2006.03.009

[22] K. Hata, D. N. Futaba, K. Mizuno, T. Namai & et al. (2004). Water-Assisted Highly Efficient Synthesis of Impurity-Free Single-Walled Carbon Nanotubes. Science, 306(5700), 1362-4.

[23] I. H. El-Sayed, X. Huang, and M. A. El-Sayed "Surface Plasmon Resonance Scattering and Absorption of anti-EGFR Antibody Conjugated Gold Nanoparticles in Cancer Diagnostics: Applications in Oral Cancer" *Nano Letters* 2005 *5* (5), 829-834

[24] Y. Sun, & Y. Xia. (2002). "Shape-controlled synthesis of gold and silver nanoparticles". Science, 298(5601), 2176-9

[25] D. C. Ralph, C. T. Black, and M. Tinkham; "Gate-Voltage Studies of Discrete Electronic States in Aluminum Nanoparticles"; Phys. Rev. Lett. Vol 78, Iss 21; 4087-4090 (1997)

[26] J. A. Eastman; S. U. S. Choi; S. Li; W. Yu; L. J. Thompson; "Anomalously increased effective thermal conductivities of ethylene glycol-based nanofluids containing copper nanoparticles", IEEE App Phy Lett; Volume: 78 Issue:6 718 – 720 Feb 2001; doi: 10.1063/1.1341218

[27] N. Wu, L. Fu, M. Su, M. Aslam, K. C. Wong, and V. P. Dravid; "Interaction of Fatty Acid Monolayers with Cobalt Nanoparticles" *Nano Letters* 2004 *4* (2), 383-386

[28] D. H. Chen and, S. H. Wu; Synthesis of Nickel Nanoparticles in Water-in-Oil Microemulsions ;*Chemistry of Materials* 2000 *12* (5), 1354-1360

[29] S. Sergei, A. Barchi, J. Joseph "De Novo Synthesis of Biofunctional Carbohydrate-Encapsulated Quantum Dots" *Frontiers in Modern Carbohydrate Chemistry.* March 13, 2007, 375-392

[30] Xu, Z. William, P. A. Charpentier; "Quantum Dots in Polymer Films for Light Selectivity"; *Functional Polymer Nanocomposites for Energy Storage and Conversion.* January 1, 2010, 137-154

[31] T.V. Hughes and C. R. Chambers, Manufacture of Carbon Filaments, US Patent No. 405, 480, (1889)

[32] M. Marc; V. Kuznetsov "Who should be given the credit for the discovery of carbon nanotubes?" Carbon 44 (9): 1621. doi:10.1016/j.carbon.2006.03.019 (2006).

[33] Figure 1.1: "Carbon." Chemicool Periodic Table taken from the website and reproduced under the GNU Free Documentation License <http://www.chemicool.com/elements/carbon.html>. accessed on 12/01/2011

[34] Data retrieved from the site: <http://www.nano.gov/about-nni/what/funding> Accessed on 12/01/2011

[35] X. Wang; Q. Li; J. Xie; Z. Jin; J. Wang; Y. Li; K. Jiang; S. Fan "Fabrication of Ultralong and Electrically Uniform Single-Walled Carbon Nanotubes on Clean Substrates". *Nano Letters* 9 (9): 3137−3141. doi:10.1021/nl901260b. PMID 19650638 (2009).

[36] J. Salvetat, G. A. D. Briggs, J. Bonard, R. R. Bacsa, A. J. Kulik, T. Stöckli, N. A. Burnham, and L. Forró; "Elastic and Shear Moduli of Single-Walled Carbon Nanotube Ropes"; Phys. Rev. Lett. 82, 944−947 (1999)

[37] B. G. Demczyk; Y. M. Wang; J. Cumings; M. Hetman; W. Han; A. Zettl; R.O. Ritchie, "Direct mechanical measurement of the tensile strength and elastic modulus of multiwalled carbon nanotubes". *Materials Science and Engineering A* 334 (1−2): 173−178. doi:10.1016/S0921-5093(01)01807-X (13 June 2002).

[38] H. Seunghun; S. Myung "Nanotube Electronics: A flexible approach to mobility". *Nature Nanotechnology* 2 (4): 207–208. doi:10.1038/nnano.2007.89. PMID 18654263

[39] G. Binnig, C. F. Quate and Ch. Gerber, "Atomic Force Microscope," *Physical Review Letters*, vol. 56, Mar. 1986, pp. 930-933.

[40] R. Saito, G. Dresselhaus, and M. Dresselhaus, *Physical Properties of Carbon Nanotubes* (World Scientific, Singapore, 1998).

[41] R. Gao, Z. L. Wang, Z. Bai, W. A. de Heer, L. Dai, and M. Gao, Phys. Rev. Lett. 85, 622 (2000).

[42] D. Li, Y. Wu, P. Kim, L. Shi, P. Yang, A. Majumdar, Thermal conductivity of individual silicon nanowires, Appl. Phys. Lett. 83 (14) (2003) 2934–2936.

[43] S. Pathak, V. B. Shenoy, Size dependence of thermal expansion of nanostructures, Phys. Rev. B 72 (2005) 113404.

[44] E. Tadmor, M. Ortiz, R. Phillips, Quasicontinuum analysis of defects in solids, Philos. Mag. A 73 (1996) 1529–1563.

[45] L. E. Shilkrot, R. E. Miller, W. A. Curtin, "Multiscale plasticity modeling: coupled atomistics and discrete dislocation mechanics", J. Mech. Phys. Solid 52 (2004) 755–787.

[46] P. A. Klein, J. A. Zimmerman, "Coupled atomistic-continuum simulation using arbitrary overlapping domains", J. Comput. Phys. 213 (2006) 86–116.

[47] F. F. Abraham, J. Broughton, N. Bernstein, E. Kaxiras, Spanning the continuum to quantum length scales in a dynamic simulation of brittle fracture, Europhys. Lett. 44 (1998) 783–787.

[48] R. E. Rudd, J. Q. Broughton, Coarse-grained molecular dynamics and the atomic limit of finite elements, Phys. Rev. B 58 (1998) 5893–5896.

[49] G. J. Wagner, W. K. Liu, Coupling of atomistic and continuum simulations using a bridging scale decomposition, J. Comput. Phys. 190 (2003) 249–274.

[50] J. Li, J. Koehne, A. M. Cassell, H. Chen, Q. Ye, H. T. Ng, J. Han and M. Meyyappan, "Miniaturized Multiplex Label-Free Electronic Chip for Rapid Nucleic Acid Analysis Based on Carbon Nanotube Nanoelectrode Arrays", 2004a. J. Mater. Chem. 14, 676-684.

[51] J. Li, J. Koehne, A. M. Cassell, H. Chen, Q. Ye, H. T. Ng, J. Han and M. Meyyappan, "Bio-Nano Fusion in Sensor and Device Development", 2004b. MCB 1 (1), 69-80.

[52] M. A. Guillorn, T. E. McKnight, A. Melechko, V. I. Merkulov, P. F. Britt, D. W. Austin, D. H. Lowndes and M. L. Simpson, "Individually Addressable Vertically Aligned Carbon Nanofiber Based Electrochemical Probes", 2002. J. Appl. Phys. 91 (6), 3824-3828.

[53] P. He and L. Dai, "Aligned Carbon Nanotube-DNA electrochemical Sensors", 2004. Chem. Commun., 348-349.

[54] Y. H. Yun, V. Shanov, M. J. Schulz, Z. Dong, A. Jazieh, W. R. Heineman, H. B. Halsall, D. K. Y. Wong, A. Bange, Y. Tuf and S. Subramaniam, "High Sensitivity Carbon Nanotube Tower Electrodes", 2006. Sens. Actuators B 120, 298-304.

[55] P. V. Gerwen, W. Laureyn, W. Laureys, G. Huyberechts, M. O. D. Beeck, K. Baert, J. Suls, W. Sansen, P. Jacobs, L. Hermans and R. Mertens, "Nanoscaled Interdigitated Electrode Arrays for Biochemical Sensors", 1998. Sensors and Actuators B, vol. 49, 73-80.

[56] F. Patolsky, G. Zheng and C. M. Lieber, 2006. "Fabrication of Silicon Nanowire Devices for Ultrasensitive, Label-Free, Real-Time Detection of Biological and Chemical Species", Nat. Protocols 1, 1711-1724.

[57] Data retrieved from the website: "http://www.nasa.gov/centers/ames/research/technology-onepagers/gas_detection.html" data retrieved on 07/06/2011

[58] E. Kolawa, " Extreme Environment technologies for future space science missions", a report by NASA; Sep 19, 2007

[59] P. M. Ajayan, L. S. Schadler, P. V. Braun (2003). *Nanocomposite science and technology*. Wiley. ISBN 3527303596

[60] A. Dawson and, P. V. Kamat "Semiconductor−Metal Nanocomposites. Photoinduced Fusion and Photocatalysis of Gold-Capped TiO2 (TiO2/Gold) Nanoparticles" *The Journal of Physical Chemistry B* 2001 *105* (5), 960-966

[61] S. K. Pillalamarri, F. D. Blum, A. T. Tokuhiro and M. F. Bertino "One-Pot Synthesis of Polyaniline−Metal Nanocomposites"*Chemistry of Materials* 2005 *17* (24), 5941-5944

[62] R. Gangopadhyay and A. De "Conducting Polymer Nanocomposites: A Brief Overview" *Chemistry of Materials* 2000 *12* (3), 608-622

[63] W. R. Schmidt, D. M. Narsavage-Heald, D. M. Jones, P. S. Marchetti,D. Raker, and G. E. Maciel "Poly(borosilazane) Precursors to Ceramic Nanocomposites" *Chemistry of Materials* 1999 *11* (6), 1455-1464

[64] X. Wang, G. Qiao and Z. Jin, Fabrication of Machinable Silicon Carbide-Boron Nitride Ceramic Nanocomposites. Journal of the American Ceramic Society, 87: 565−570. doi: 10.1111/j.1551-2916.2004.00565.x

[65] G. Guisbiers and L. Buchaillot, "Universal Size/Shape-Dependent Law for Characteristic Temperatures, 2009, Physics Letters A, 374:305.

[66] E. Pop, D. A. Mann, K. E. Goodson, H. Dai; "Electrical and Thermal Transport in Metallic Single-Wall Carbon Nanotubes on Insulating Substrates" Journal of Applied Physics 101, 093710 (2007)

[67] M. A. Kuroda, A. Cangellaris, and J. Leburton; "Nonlinear Transport and Heat Dissipation in Metallic Carbon Nanotubes" Phys. Rev. Lett. 95, 266803 (2005)

[68] M. Suzuki, Y. Ominami, Q. Ngo, C. Y. Yang, A. M. Cassell, and J. Li; "Current-induced breakdown of carbon nanofibers" J. Appl. Phys. 101, 114307 (2007); doi:10.1063/1.2743086

[69] Q. Ngo, A. M. Cassell, A. J. Austin, J. Li, S. Krishnan, M. Meyyappan and C. Y. Yang, "Characteristics of aligned carbon nanofibers for interconnect via applications" IEEE Electron Device Lett. 27, 221 (2006)

[70] C. A. Schuh, T. G. Nieh, A nanoindentation study of serrated flow in bulk metallic glasses, Acta Materialia, Volume 51, Issue 1, 8 January 2003, Pages 87-99

[71] P. K. Zysset, X. E. Guo, C. E. Hoffler, K. E. Moore, S. A. Goldstein, Elastic modulus and hardness of cortical and trabecular bone lamellae measured by nanoindentation in the human femur, Journal of Biomechanics, Volume 32, Issue 10, October 1999, Pages 1005-1012, ISSN 0021-9290, DOI: 10.1016/S0021-9290(99)00111-6.

[72] B. J. Briscoe et al 1998 J. Phys. D: Appl. Phys. 31 2395 doi: 10.1088/0022-3727/31/19/006

[73] L. Dong; C. Yip Wah; W. Ming Show; S. D. William.; "Nanoindentation studies of ultrahigh strength carbon nitride thin films," Journal of Applied Physics , vol.74, no.1, pp.219-223, Jul 1993 doi: 10.1063/1.355304

[74] A. Gouldstone, H. J. Koh, K. Y. Zeng, A. E. Giannakopoulos, S. Suresh, Discrete and continuous deformation during nanoindentation of thin films, Acta Materialia, Volume 48, Issue 9, 29 May 2000, Pages 2277-2295, ISSN 1359-6454, DOI: 10.1016/S1359-6454(00)00009-4.

[75] AFM probe model: Tap190DLC, BudgetSensors, Innovative Solutions Bulgaria Ltd., Sofia, Bulgaria.

[76] I. N. Sneddon, "The relation between load and penetration is the axisymmetric boussinesq problem for a punch of arbitrary profile". International Journal of Engineering Science, vol. 3, issue 1, pp. 47-57, 1965.

[77] L. J. Hall, V. R. Coluci, D. S. Galvão, M. E. Kozlov, M. Zhang, S. O. Dantas, R. H. Baughman; "Sign Change Of Poisson's Ratio For Carbon Nanotube Sheets" Science; Vol 320; 504-507; 25 April 2008

[78] Y. Min-Feng; L. Oleg; D. Mark J.; M. Katerina; Kelly, Thomas F.; Ruoff, Rodney S. (28 January 2000). "Strength and Breaking Mechanism of Multiwalled Carbon Nanotubes Under Tensile Load". Science 287 (5453): 637–640. doi:10.1126/science.287.5453.637

[79] B. Peng, M. Locascio, P. Zapol, S. Li, S. L. Mielke, G. C. Schatz, and H. D. Espinosa, "Measurements of near-ultimate strength for multiwalled carbon nanotubes and irradiation-induced crosslinking improvements," Nature Nanotechnology, vol. 3, pp. 626 – 631, 2008.

[80] P. M. Ajayan, O. Stephan, C. Colliex, D. Trauth, Science 265 (1994) 1212.

[81] A. K. Wanekaya, Y. Lei, E. Bekyarova, W. Chen, R. Haddon, A. Mulchandani, N. V. Myung, Electroanalysis 18 (2006) 1047.

[82] X. Zhang, J. Zhang, Z. Liu, Carbon 43 (2005) 2186.

[83] P. A. Fontaine, E. Dubois and D. Stievenard, "Characterization of scanning tunneling microscopy and atomic force microscopy-based techniques for nanolithography on hydrogen-passivated silicon," *Journal of Applied Physics*, vol. 84, no. 4, Aug. 1998, pp. 1776-1881.

[84] Z. Q. Wang, N. D. Jiao, S. Tung and Z. L. Dong, "Atomic force microscopy-based repeated machining theory for nanochannels on silicon oxide surfaces," *Applied Surface Science*, 257 (2011), pp. 3627-3631

APPENDIX A: DESCRIPTION OF RESEARCH FOR POPULAR PUBLICATION

Physiochemical and Nanomanipulation of Carbon Nanomaterials

By Siva Naga Sandeep Chalamalasetty

Imagine a rover that was built using billions of dollars, was sent to new unexplored lands millions of miles away from its home. Can you digest the fact that after the rover's successful lauch, journey and landing, it undergoes a malfunction in its sensory system and cannot be used anymore? Though you might feel this as an exaggeration, after taking a look at the report released by NASA in 2008, you will understand that it is a hard to digest fact. There is even a high probability that this mistake might repeat if we don't learn from mistakes causing failures. Material researcher Sandeep Chalamalasetty set forward to solve this problem by studying the material behavior by stimulating the extreme environments that might prevail in the outer space. Thanks to the commitment of Dr. Uche Wejinya for developing Micro and Nano Sytems Engineering research lab. In this regard Dr. Wejinya says "With knowing the reliability of the material, there is always a scope to build a better sensory system"

Much of our knowledge on the materials we use is based on their terrestrial behavior.But materials resond to the environments surrounding them including temperature, pressure, radiation, different chemicals etc. The material behavior in the extreme environments is the unseen source for the failure of prior NASA space exploration missions. Therefore, it can be concluded that material behavior is a serious design consideration.

With its amazing physiochemical, optoelectronic and mechanical properties bundled with light weight, carbon nanomaterials had attracted huge attention of the scientific community. Billions of dollars investment, flexibility of the material had expanded the horizon of the carbon nanomaterials in the fields of electronics, communications, biomedical and aerospace. The above said properties had made the carbon nanomaterials ideal for aerospace applications. Dr. Wejinya emphasizes on the reliability studies of nanomaterials given their tremendous potential of applications in the fields of science and industry.

As material behavior in the extreme environments became a serious design consideration and owing to the vast research that is being done on carbon nanomaterials in the field of aerospace, researchers of Micro Nano Systems Engineering lab at University of Arkansas in collaboration with NASA Ames research center had characterized the behavior of carbon nanofibers in extreme environments. The research on the extreme environmental behavior was followed by a rudimentary research on the effect of acidic corrosive substance on the carbon nanofibers. The current results could be used for design considerations involving the carbon nanomaterials.

APPENDIX B: EXECUTIVE SUMMARY OF NEWLY CREATED INTELLECTUAL PROPERTY

The following list of new intellectual property items were created in the course of this research project and should be considered from both a patent and commercialization perspective.

1. A method for measuring the mechanical properties of materials that are smaller than 200 nm in dimension. This approximation technique can be further refined for measurement of mechanical properties of materials that are much smaller than 200 nm.
2. A new nanocomposite based on conductive polymer and carbon nanotube was developed.

APPENDIX C: POTENTIAL PATENT AND COMMERCIALIZATION ASPECTS OF LISTED INTELLECTUAL PROPERTY ITEMS

C.1 Patentability of Intellectual Property (Could Each Item be Patented)

The two items listed were considered first from the perspective of whether or not the item could be patented.

1. The method developed for the measurement of mechanical properties can be patented. But since this method was based on the previously done works on the materials at nanoscale, it is unclear whether such a patent can be pursued.
2. New nanocomposites with better electrical resistance developed can be patented. However, it is unclear at this time, whether such a work was done previously or not.

C.2 Commercialization Prospects (Should Each Item Be Patented)

The two items listed were then considered from the perspective of whether or not the item should be patented.

1. With materials dimensions shrinking day to day, it is becoming harder for the researchers and industries to find effective methods for measurement of material properties. Hence, the method for measuring the mechanical properties at nanoscale can be successfully commercialized.
2. New nanocomposites developed should be patented and then commercialized for better nanomaterials integration.

C.3 Possible Prior Disclosure of IP

The following items were discussed in a public forum or have published information that could impact the patentability of the listed IP.

1. All of the two items afore mentioned were in the preliminary stage of development and no patent can be filed on these items at this point of time.

APPENDIX D: BROADER IMPACT OF RESEARCH

D.1 Applicability of Research Methods to Other Problems

For the first time, nanoindentation had been effectively used for calculation of the Young's modulus of nanomaterials which are smaller than 200 nm in length. This approach can be adapted into future research works using AFM. Nanocomposites are synthesized using the elctropolymerization and this can be used for synthesis of other novel nanocomposites. picoLITH had been effectively used for creation of nanochannels which are less than 10nm deep. Dielectrophoretic movement which was used for movement of nanocomposites, SWCNTs and MWCNTs can be applied for movement of any polarizable compounds in between the electrodes.

D.2 Impact of Research Results on U.S. and Global Society

The present research results will aid in the development of novel Micro Electro Mechanical Systems (MEMS) which are capable of high speed electron transfers and thus can find application in the areas of Sensing, Electronics and futuristic MEMS. Since sensing is largely dependent on the resistance of the carbon nanomaterials, nanocomposites, which have a resistance 40 fold less than the actual CNT can enormously increase the sensing capabilities of an electrochemical biosensor.

D.3 Impact of Research Results on the Environment

This research method does not have any adverse environmental impact from the manufacture of the materials and devices.

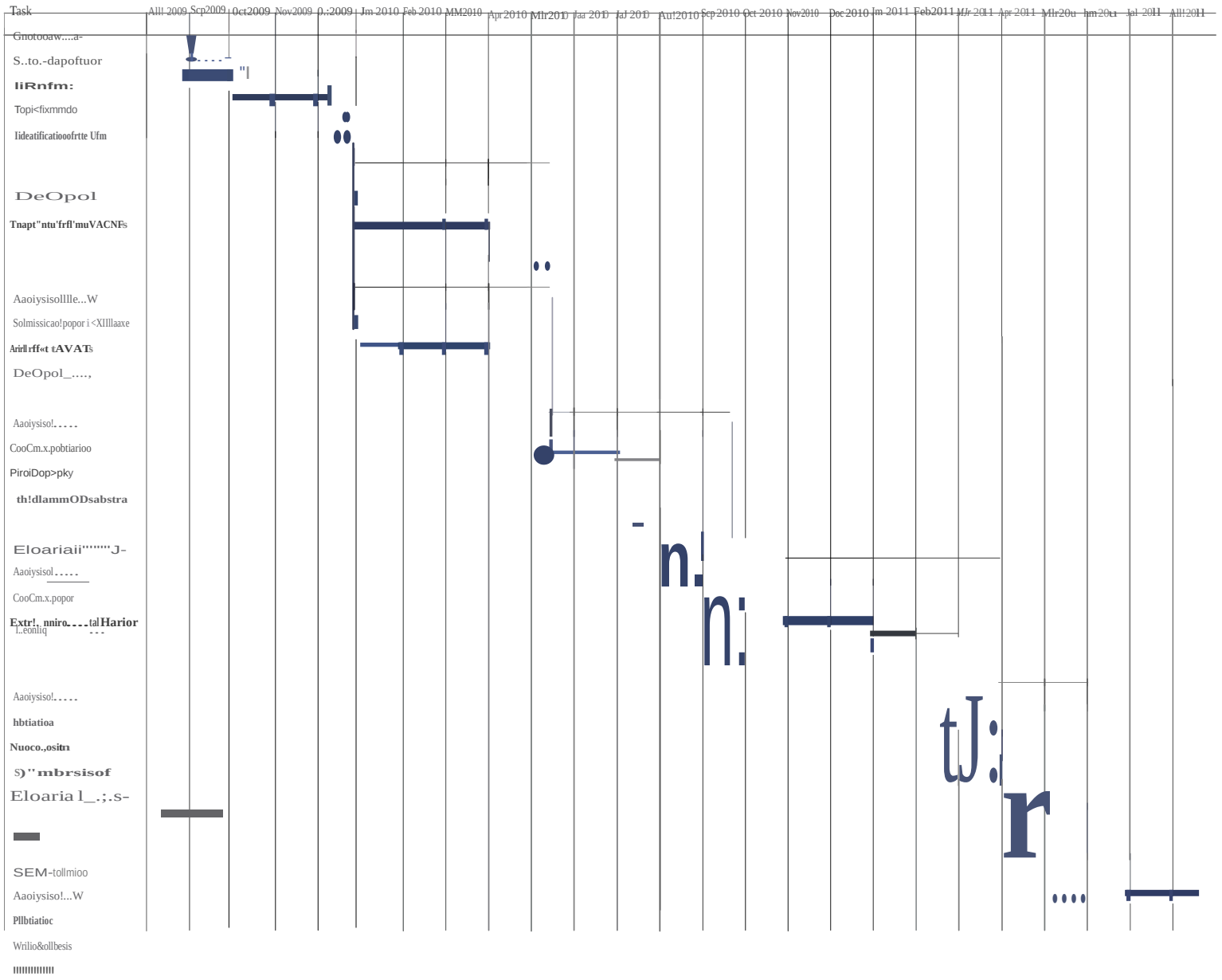
Task
Gnotooaw....a-
S..to.-dapoftuor
liRnfm:
Topi<fixmmdo
Iideatificatiooofrtte Ufm
DeOpol
Tnapt"ntu'frfl'muVACNFs
Aaoiysisolllle...W
Solmissicao!popor i <XIIIlaaxe
Aridlrff«t tAVATs
DeOpol_....,
Aaoiysiso!.....
CooCm.x.pobtiarioo
PiroiDop>pky
th!dlammODsabstra
Eloariaii"""""J-
Aaoiysisol.....
CooCm.x.popor
Extr!, nniro.....tal Harior
Aaoiysiso!.....
hbtiatioa
Nuoco.,ositn
s)"mbrsisof
Eloaria l_.;.s-
SEM-tollmioo
Aaoiysiso!...W
Pllbtiatioc
Wrilio&ollbesis
IIIIIIIIIIIII

APPENDIX F: IDENTIFICATION OF ALL SOFTWARE USED IN RESEARCH AND THESIS/DISSERTATION GENERATION

Computer #1:
- Model Number: Dell Dimension 8300
- Location: ENRC 3917
- Owner: Dr. Uchechukwu C. Wejinya

Software #1:
- Name: Microsoft Office 2007
- Purchased by: UA Mechanical Engineering Dept.

Software #2:
- Name: MATLAB v6.5
- Purchased by: UA Mechanical Engineering Dept.

Software #3:
- Name: Adobe Acrobat Professional 10.0
- Purchased by: University of Arkansas Site License

Software #4:
- Name: Picoview AFM imaging software
- Purchased by: Dr. Uchechukwu C. Wejinya

Computer #2:
- Model Number: emachines EL 1200-06w
- Serial Number: PTNAE050158450C51F3001
- Location: Personal
- Owner: Sandeep Chalamalasetty

Software #1:
- Name: Microsoft Project 2003
- Purchased by: University of Arkansas Site License.

Software #2:
- Name: Adobe Acrobat Reader X
- Purchased by: Adobe Site License

APPENDIX G: ALL PUBLICATIONS PUBLISHED, SUBMITTED AND PLANNED

- **Journal Publications:**
  - *"Dimensional Analysis and Mechanical Properties Characterization of Carbon Nanofibers under Subzero Temperatures"* under review, Nature Nanotechnology
  - *"Carbon Nanofibers Nanoelectrode Array: Effect of process conditions on reliability"* in Press TNANO, IEEE
  - *"Development of CNT-ISFET based pH sensing system using Atomic Force Microscopy – A preliminary study"* in Press, Journal of Sensors and Actuators: A Physical
  - *"The effect of Acids on Carbon Nanofibers (CNFs) for Chemical Sensor development"* under review, TNANO,IEEE
  - *"Synthesis and electrochemical characterization of conductive polymer – carbon nanotube nanocomposites"*, under review, Journal of Nanostructured polymers and Nanocomposites
- **Conference Publications:**
  - "*Characterization of etched and unetched vertically aligned carbon nanofibers"* published at IEEE IROS 2010.
  - "*A study of Temperature effect on Vertically Aligned Carbon Nanofibers for Bio/Chemical Sensor development"* published at IEEE NANO 2010
  - *"Acid Etch Study of Vertically Aligned Carbon Nanofibers"* published at IEEE NMDC 2010.
  - *"A study of Temperature effect on Etched and Unetched Vertically Aligned Carbon Nanofibers"* published at IEEE ROBIO 2010.
  - "*Atomic force microscopy based Nanomanipulation for CNT-ISFET based* pH *sensor"* IEEE NEMS 2011
  - "*A study Effect of sulfuric and acetic acid on the Vertically Aligned Carbon Nanofibers (VACNFs) for chemical sensor development"* IEEE NANO 2011

APPENDIX G: FABRICATION PROCEDURE OF VERTICALLY ALIGNED CARBON NANOFIBERS (VACNFS) NANO ELECTRODE ARRAYS

The procedure given below was the direct quote of the fabrication steps actually done at NASA Ames Research Center by *P. Armugam et al* and was previously published in journal of Biosensors and Bioelectronics.

(1) Optical lithography patterning of micro pads, contact pads and electrical interconnects:

A single 4-in. wafer consists of 30 chips. Each chip contains nine micro pad arrays (3×3 format, 200 μm squares) connected to nine contact pads (1mm squares). The underlying oxide electrically isolates all nine micro pads. The pads and interconnects were patterned using a 1μm thick Shipley 3612 resist and microlithography. (*Caution*: Photoresists are irritants. Avoid long-time exposure or inhalation). Following inspection in an optical microscope, the patterns were metalized using a liftoff technique. A 200 nm thick Cr film was deposited by electron beam evaporation. The coated wafers were immersed in acetone for 1 h. The wafers were then removed from the acetone while being sprayed with methanol and isopropyl alcohol (IPA). Finally, the wafers were blown dry with N_2.

(2) Electron beam lithography patterning of catalyst dots on micro pads):

A single micro pad consists of ~39,000 catalyst dots. Each dot was 100 nmdiameter. A 400 nm thick Poly (methylmethacrylate) (PMMA) A7was spun coated at 3000 rpm, baked at 180°C for 90 s, and exposed at 100 keV, 2 nA, 1950 μC/cm^2. The exposures were developed in a solution of 1:1methyl isobutyl ketone (MIBK): IPA for 2min, immersed in IPA for 30 s, and blown dry with N_2. Following inspection under an optical microscope, the patterns were metalized using a liftoff technique. A 10 nm Cr followed by 30 nm Ni catalyst were deposited by

electron beam evaporation at ~2 Å/s. The coated wafers were immersed in acetone for 1 h. The wafers were then removed from the acetone while being sprayed with IPA and then blown dry with N_2.

(3) DC-biased PECVD growth of VACNFs on the nickel dots:

C_2H_2 feedstock (125 sccm) and NH_3 diluent (444 sccm) were used at a processing pressure of 6.3 mbar, temperature of 700°C and the plasma power of 180W. A 5 min thermal annealing at 600°C was performed before initiating the plasma with 250 sccmNH_3. A 60°C/min thermal ramp was used to reach both the thermal anneal and growth temperatures. Each CNF was vertically aligned and freestanding on the surface with Ni catalyst at the tip. A 15 min deposition yielded, on average, a height of 1.5μm, a base diameter of 100 nm, and a tip diameter of 70 nm. During initial optimization, the uniformity of VACNF growth was checked by SEM.

(4) PECVD of silicon dioxide:

A 3μm±0.8% SiO_2 layer was deposited onto the wafers to passivate the sidewalls of the fibers. A mixture of O_2 (~6000 sccm) and TEOS (2−3 ml/min) was used in a parallel plate, dual RF, PECVD to create a highly conformal coating on the high aspect ratio fibers and interconnects. The process temperature, pressure and RF power were 400°C, 3 Torr and 1000 W, respectively.

(5) Re-exposure of VACNF tips and surface planarization:

The excess oxide and part of the VACNFs were removed by CMP. The CMP consists of two steps, stock removal and final polish. A 0.5μm alumina (pH 4) at 10 ml/min, 60-rpm platen, 15-rpm carrier, and 15 psig down force was used to remove bulk material at ~150 nm/min. A 0.1μm alumina (pH 4) at 10 ml/min, 60-rpm platen, 15-rpm carrier, and 25 psig down force was

used for final polish at ~20 nm/min. The wafers were cleaned in a mixture of water, hydrogen peroxide and ammonium hydroxide (80:2:1) and spin-dried.

(6) Selective etching of silicon dioxide to expose the contact pads:

Selective removal of SiO2 from the contact pads for electrical connections to the potentiostat was defined by optical lithography using a 2.5 μm thick Shipley 3012 resist. The resist was soft baked at 125°C for 120 s, exposed and developed in Shipley EC 11 for 1 min. After a 5 min rinsing with deionized (DI) water and inspection with an optical microscope, the resist was hard baked at 125°C for 180 s. A 7:1 diluted HF solution was used to selectively etch the oxide at ~15 Å/s (*Caution*: HF is an extremely hazardous liquid and vapor, and is highly corrosive to eyes and skin. Goggles and gloves must be used during operation). The resist was stripped using EKC 830 resist stripper in 15 min. Following rinsing with DIwater and blown dry with N_2, the wafers were diced into individual chips of ~14mm squares in size.